arXiv:hep-ph/0307244v2 26 Sep 2003

ICARUS-TM/03-03
July 18, 2003
Revised February 7, 2008

Oscillation effects on supernova neutrino rates and spectra and detection of the shock breakout in a liquid Argon TPC

I. Gil-Botella[1], A. Rubbia[2]

Institut für Teilchenphysik, ETHZ, CH-8093 Zürich, Switzerland

Abstract

A liquid Argon TPC (ICARUS-like) has the ability to detect clean neutrino bursts from type-II supernova collapses. In this paper, we consider for the first time the four possible detectable channels, namely, the elastic scattering on electrons from all neutrino species, ν_e charged current absorption on Ar with production of excited K, $\bar{\nu}_e$ charged current absorption on Ar with production of excited Cl and neutral current interactions on Ar from all neutrino flavors. We compute the total rates and energy spectra of supernova neutrino events including the effects of the three–flavor neutrino oscillation with matter effects in the propagation in the supernova. Results show a dramatic dependence on the oscillation parameters and in the energy spectrum, especially for charged-current events. The shock breakout phase has also been investigated using recent simulations of the core collapse supernova. We stress the importance of the neutral current signal to decouple supernova from neutrino oscillation physics.

[1]Ines.Gil.Botella@cern.ch
[2]Andre.Rubbia@cern.ch

1 Introduction

Core collapse supernovae are a huge source of all flavor neutrinos. Neutrino astrophysics entered a new phase with the detection of neutrinos from the supernova SN1987A in the Large Magellanic Cloud by the Kamiokande and IMB detectors [1]. In spite of these fundamental neutrino observations, the 19 events observed are not statistically significant enough to obtain precise quantitative information on the neutrino spectrum. Currently running neutrino detectors like Superkamiokande or SNO have the capabilities to provide high statistics information about supernova and neutrino properties if a supernova collapse were to take place in the near future.

The flavor composition, energy spectrum and time structure of the neutrino burst from a galactic supernova can give information about the explosion mechanism and the mechanisms of proto neutron star cooling. In addition, because neutrinos arrive before any other signal from a supernova, it is possible to provide an early alert to the astronomical community combining the observations of several experiments. This will allow an early observation of the first stages of the supernova explosion.

The neutrino signal from a galactic supernova can also give information about the intrinsic properties of the neutrino such as flavor oscillations. Although new data from solar, atmospheric, reactor and accelerator neutrinos [2] have contributed to the understanding of the neutrino properties, still the neutrino mixing angle θ_{13} and the nature of the mass hierarchy, i.e., normal or inverted, remain unknown. These parameters can be probed by the observation of supernovae neutrino bursts, since neutrinos will travel long distances before reaching the Earth and will, as they travel through the exploding star, in addition traverse regions of different matter densities where matter enhanced oscillations will take place. In the case of the θ_{13} angle, matter enhancement has the striking feature that very small mixing angles, beyond any value detectable by next generation accelerators, could in fact alter significantly the neutrino spectrum. Hence, supernova neutrinos provide indeed a complementary tool to study the θ_{13} angle.

The main question of course is to understand to which extend can the supernova and the neutrino physics be decoupled in the observation of a single supernova? On one hand, the understanding of the supernova explosion mechanism is still plagued by uncertainties which have an impact on the precision with which one can predict time, energy and flavor-dependent neutrino fluxes. On the other hand, the intrinsic neutrino properties are not fully known, since the type of mass hierarchy and the value of the θ_{13} angle are unknown, and in fact large uncertainty still exist on the prediction of the actual effect of neutrino oscillation.

There have been various studies on future supernova neutrino detection and their interplay with neutrino oscillations physics. Dighe and Smirnov [3] estimated qualitatively the effects of neutrino oscillations in a collapse-driven supernova on the neutronization peak, the distortion of energy spectra and the Earth matter effect. Dutta et al [4] and also Takahashi et al [5] showed numerically that the total number of events for Superkamiokande and SNO detectors increases dramatically when there is neutrino mixing.

Detailed supernova simulations (see e.g. [6]) indicate that the average neutrino energy is flavor dependent and hierarchical ($E_{\nu_e} < E_{\bar{\nu}_e} < E_{\nu_{\mu,\tau},\bar{\nu}_{\mu,\tau}}$). Great uncertainties still exist in the spectral and temporal evolution of the neutrino fluxes. Although the hierarchy of the average energies of the ν_e, $\bar{\nu}_e$ and ν_x, $\bar{\nu}_x$ is believed to hold, quantitatively their specific spectra remain a matter of detailed calculations (see [7], and [8] and references therein). Under the assumption of hierarchical neutrinos, neutrino flavor oscillations should make the spectra of ν_e and $\bar{\nu}_e$ harder (see [9] and references therein). This will lead to a change in the neutrino observations in the detector because the cross sections depend strongly on the neutrino energy and they are different for different flavors.

It is hence well known that uncertainties in the supernova explosion mechanism and the effect of neutrino oscillations can change dramatically the number of observed events in a given experiment. Indeed, this dependence can be used to determine the supernova and mixing parameters, once the next supernova has been detected. Most detailed studies in the literature however concern water or heavy-water targets (see e.g. [10, 11, 12, 13]). In addition, some authors advocate the use of specific variables in order to disentangle supernova from neutrino oscillation physics (see e.g. [9]).

In this work we study the capabilities of a liquid Argon TPC (ICARUS-like) to detect neutrinos from supernova collapses and its possible contributions to this field. Our study is motivated by the proposed 3 kton ICARUS detector [14] that should become operational at the Gran Sasso Underground Laboratory and by ideas for a very large liquid Argon TPC with a mass in the range of 100 kton's (see e.g. [15]).

We think that a liquid Argon detector has excellent potentialities for supernova physics, namely because of its high granularity and bubble-chamber like features, all channels, namely elastic scattering off atomic electrons, as well as charged and neutral nuclear scattering processes are detectable and identifiable. The simultaneous observation of nuclear charged and neutral currents provide high-statistics and golden channels to decouple supernova from neutrino oscillation physics.

It is known that precise elastic scattering can also yield information on the flavor content of the flux (see e.g. [2] in the context of the solar neutrino puzzle), because of different cross-sections depending on flavor and helicity. However, this requires good statistical precision that is more difficult to achieve with target electrons than with nuclear target. Hence, nuclear processes are expected to contribute most.

A Liquid Argon TPC can also separate the various channels by a classification of the associated photons from the K, Cl or Ar de-excitation, which exhibit specific spectral lines, or by the absence of associated photons in case of the elastic scattering. It is hence possible to detect ν_e, $\bar{\nu}_e$ and other flavors independently.

In section 2, we briefly recall the general framework we used in this study. In particular, we identify five scenario for the cooling of the supernova. Neutrino oscillations in vacuum and in the supernova matter are discussed in section 3.

In section 4, we discuss the relevant neutrino cross-section on Argon and identify the experimentally detectable classes of events. New calculations on the cross section

for the absorption processes based in the random phase approximation (RPA) were used allowing computing for the first time the contribution of the $\bar{\nu}_e$ ^{40}Ar absorption reaction and of neutral current reactions.

In section 5, a particular interest is taken on detection of the early phase neutrino signal from supernova in liquid Argon. We investigate the expected events coming from the first hundreds of milliseconds after the supernova bounce using the calculations on the shock breakout process in core collapse supernovae and taking neutrino oscillations into account.

In section 6, we compute the expected neutrino rates in liquid Argon, for different primary supernova neutrino fluxes scenarios. Moreover, the energy spectra modified by oscillations are plotted for different conditions on the oscillation parameters. From supernova neutrino observations it is possible to extract information about the character of the mass hierarchy and the θ_{13} mixing angle.

2 General framework and supernova explosion scenarios

When the iron core of a massive star ($M \geq 8$ $M_\odot$) overcomes its hydrodynamical stability limit (the Chandrasekhar mass), the core collapses raising its density up to many times the nuclear density. During this infall stage of the collapse, a first ν_e burst is emitted ("*infall burst*"), since the high density of matter enhances the electron capture by protons. The total energy radiated during this phase is roughly 10^{51} ergs.

This emission does not continue indefinitely, since at a density $\sim 10^{12}$ g cm^{-3} neutrinos are trapped in the stellar core and go to equilibrium with matter. The anomalous density produces an elastic bounce of the core, which results in a shock wave. After the *core bounce*, also neutrinos of other flavors begin to be produced. The neutrinos are trapped in a region ("neutrinosphere") whose size is different for different neutrino flavors. A deeper neutrinosphere corresponds to a higher temperature.

The wave propagates through the star and loses energy in dissociating nucleons. When the shock crosses the ν_e neutrinosphere, an intense burst of ν_e ("*shock breakout*" or "*neutronization burst*") is produced by electron capture on the large number of protons liberated by the shock. The characteristic time of the breakout burst is 3–10 ms and the total energy radiated in ν_e neutrinos during breakout is $\sim 3 \times 10^{51}$ ergs.

After the breakout stage, the ν_e luminosity rapidly decreases, while the luminosities of other flavor neutrinos increase. At the end of the neutrino diffusion inside the mantle the energy is practically equally distributed between the various neutrino flavors. The shock wave stalls without driving off the stellar mantle and envelope. ν_e and $\bar{\nu}_e$ are absorbed on the nucleons liberated by the shock. Such processes supply new energy to the wave, which is revived ~ 500 ms after the bounce. This energy transfer is known as "neutrino heating". Continued mass accretion and convection below the shock wave

also deposit energy ans thus contribute to the shock revival. The reinforced shock can propagate within the stellar matter and expel the external layers into the space.

After the explosion the star loses energy, mainly by neutrino emission, and cools down, forming a neutron star or a black hole. This final stage ("*cooling*") requires $\sim$ 10 s and takes away > 99 % of the gravitational energy of the star ($\sim$ 2–4 $\times$ 10^{53} ergs).

In order to obtain quantitative estimates, the following general considerations are taken into account for the present analysis:

- SN type-II at a distance of 10 kpc (galactic supernovae)
- Gravitational binding energy of 3×10^{53} ergs (radiated away as neutrinos).

In our analysis of the event rates and energy spectra, we simplify the supernova neutrino emission process and assume that it can be split into two distinct phases: the early ν_e pulse expected in the first 40 ms of the collapse (*shock breakout*) and the rest beyond the first 40 ms which we treat as a *cooling stage*, which could in reality last up to $\sim$ 10 s.

- For the shock breakout we use the time-dependent energy spectra from Burrows et al. The calculation is based on dynamical models of core collapse supernovae in one spatial dimension, employing a newly-developed Boltzmann neutrino radiation transport algorithm, coupled to Newtonian Lagrangean hydrodynamics and a consistent high-density nuclear equation of state. Full details of the simulation can be found in [16]. Recent studies on the initial mass progenitor dependence seem to indicate that the major features of the early neutrino burst should be almost independent of the initial mass of the star [8].
- For the cooling stage we assume that the energy spectra of neutrinos is a Fermi-Dirac distribution. In order to take into account the uncertainties in the modelling of the cooling phase, we consider five different scenarios which correspond to simulations found in the literature. The various scenarios can be parameterized by different assumptions on the average energies and relative luminosities of the different neutrino flavors. Table 1 summarizes the different possibilities for the primary supernova neutrino flux parameters and neutrino average energies considered in this work.

We assume the following neutrino oscillation situations:

- Normal ($m_1^2 < m_2^2 << m_3^2$) and inverted ($m_3^2 << m_1^2 < m_2^2$) mass hierarchies are investigated in the analysis.
- Matter effects inside the supernova are included.
- The following neutrino oscillations parameters are used in the analysis, obtained from other neutrino observations [2]:

$$\begin{array}{ll} \sin^2 2\theta_{23} = 1. & \Delta m^2_{32} \approx \Delta m^2_{31} = 3 \times 10^{-3} eV^2 \\ \sin^2 \theta_{12} = 0.3 & \Delta m^2_{21} = 7 \times 10^{-5} eV^2 \\ \sin^2 \theta_{13} < 0.02 & \end{array} \quad (1)$$

Cooling scenario	$\langle E_{\nu_e} \rangle$ MeV	$\langle E_{\bar{\nu}_e} \rangle$ MeV	$\langle E_{\nu_{\mu,\tau}} \rangle = \langle E_{\bar{\nu}_{\mu,\tau}} \rangle$ MeV	Luminosity	Reference
I	11	16	25	$L_{\nu_e} = L_{\bar{\nu}_e} = L_{\nu_x}$	[17]
II	13	16	23	$L_{\nu_e} = L_{\bar{\nu}_e} = L_{\nu_x}$	[10]
III	13	16	17.6	$L_{\nu_e} = L_{\bar{\nu}_e} = L_{\nu_x}$	[7, 18]
IV	13	16	17.6	$L_{\nu_e} = L_{\bar{\nu}_e} = 2L_{\nu_x}$	[7, 18]
V	13	16	17.6	$L_{\nu_e} = L_{\bar{\nu}_e} = 0.5\ L_{\nu_x}$	[7, 18]

Table 1: Supernova cooling phase scenarios.

3 Neutrino oscillations and matter effects

Neutrinos produced in the high density region of the iron core interact with matter before emerging from the supernova. Due to the non-zero masses and non-zero vacuum mixing angles among various neutrino flavors, flavor conversions can occur in supernovae.

The transitions are produced mainly in the so-called resonance layers. The resonance density can be computed as [3]:

$$\rho_{res} \approx \frac{1}{2\sqrt{2}G_F} \frac{\Delta m^2}{E} \frac{m_N}{Y_e} cos2\theta \tag{2}$$

where G_F is the Fermi constant, Δm^2 is the mass squared difference, θ is the mixing angle, E is the neutrino energy, m_N is the nucleon mass and Y_e is the number of electrons per nucleon.

Since the inner supernova core is too dense to allow resonance conversion, we can consider two resonance points in the outer supernova envelope: one at high density $\rho \approx 10^3$–10^4 g cm^{-3} (**H–resonance**) which is governed by the atmospheric parameters (Δm^2_{31} and θ_{13}) and the other one at low density $\rho \approx$ 10–30 g cm^{-3} (**L–resonance**), characterized by the solar parameters (Δm^2_{21} and θ_{12}).

The transitions in the two resonance layers can be considered independently and each transition is reduced to a two neutrino oscillation problem. The H–resonance lies in the neutrino channel for normal mass hierarchy and in the antineutrino channel for the inverted hierarchy. The L–resonance lies in the neutrino channel for both the hierarchies [3].

The probability of transition between one neutrino eigenstate to another in the resonance layer (L or H) is called *jump probability* (P_L or P_H).

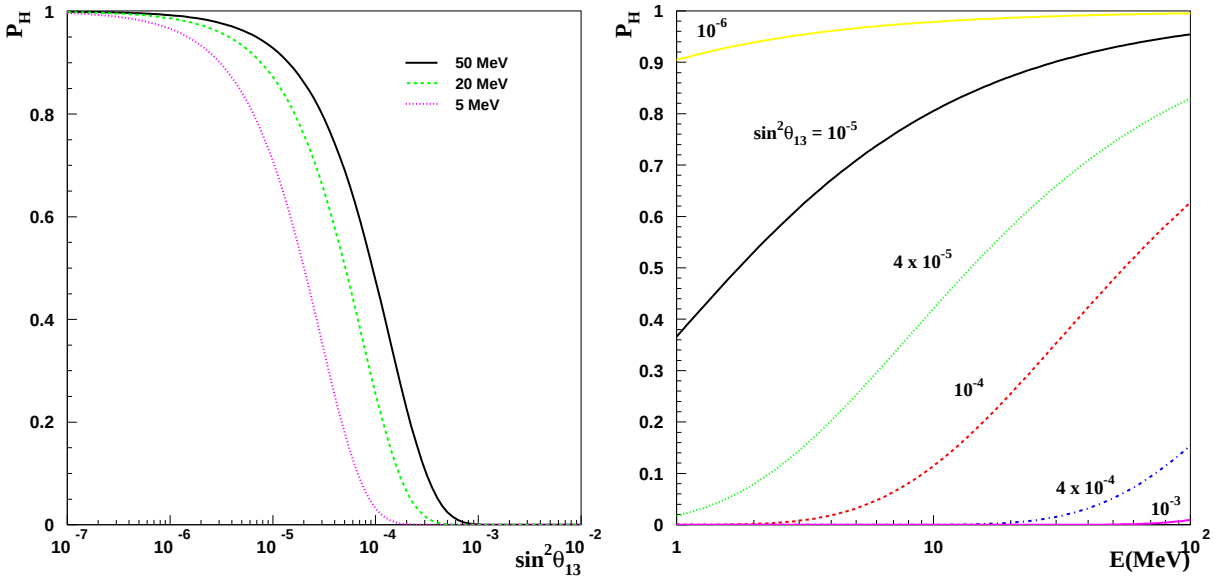

Figure 1: Jump probability in the H-resonance, P_H, as a function of $\sin^2\theta_{13}$ for three values of the neutrino energy (left), and as a function of the neutrino energy for different values of $\sin^2\theta_{13}$ (right).

The propagation through the low density region is always adiabatic for the LMA solar parameters. It means that P_L and $\overline{P}_L$ are both equal to 0 and the neutrino mass eigenstates remain unchanged.

Considering a matter density profile of the star $\rho(\mathrm{r}) \propto \mathrm{r}^{-3}$, the jump probability in the H-resonance can be written as [3]:

$$P_H \propto \exp\left[-const\ \sin^2\theta_{13}\left(\frac{\Delta m^2_{31}}{E}\right)^{2/3}\right] \tag{3}$$

Indeed, the neutrino conversion in the high density region depends on the mixing angle θ_{13} and the mass squared difference between the involved flavors, as shown in figure 1. The variation of the jump probability with the 13-mixing angle and the neutrino energy is plotted. We see that the crossing probability increases with energy. Three regions can be distinguished:

1. *Non adiabatic region* ($\sin^2\theta_{13} < 2 \times 10^{-6}$): For these values of θ_{13} the jump probability is almost equal to 1, independently of the neutrino energy.

2. *Intermediate region* ($2 \times 10^{-6} < \sin^2\theta_{13} < 3 \times 10^{-4}$): In this region the value of P_H, between 0 and 1, depends on θ_{13} and neutrino energy as expressed in the equation 3.

3. *Adiabatic region* ($\sin^2\theta_{13} > 3 \times 10^{-4}$): The jump probability is equal to 0 for any value of the neutrino energy. Then, there is no conversion between eigenstates in the resonance layer.

The effect of oscillations in the neutrino fluxes is summarized in equation 4, where the expected fluxes at the detector (ϕ_ν) are computed in terms of the original fluxes at the SN core (ϕ^o_ν) and the survival probabilities $\mathrm{P}_{ee} = \mathrm{P}(\nu_e \to \nu_e)$ and $\overline{P}_{ee} = \mathrm{P}(\bar{\nu}_e \to \bar{\nu}_e)$[1]:

$$\begin{array}{l} \phi_{\nu_e} = \phi^o_{\nu_e} P_{ee} + \phi^o_{\nu_x}(1 - P_{ee}) \\ \phi_{\bar{\nu}_e} = \phi^o_{\bar{\nu}_e} \overline{P}_{ee} + \phi^o_{\bar{\nu}_x}(1 - \overline{P}_{ee}) \\ \phi_{\nu_\mu} + \phi_{\nu_\tau} = \phi^o_{\nu_e}(1 - P_{ee}) + \phi^o_{\nu_x}(1 + P_{ee}) \\ \phi_{\bar{\nu}_\mu} + \phi_{\bar{\nu}_\tau} = \phi^o_{\bar{\nu}_e}(1 - \overline{P}_{ee}) + \phi^o_{\bar{\nu}_x}(1 + \overline{P}_{ee}) \end{array} \tag{4}$$

with $\phi^o_{\nu_x} = \phi^o_{\nu_\mu} = \phi^o_{\nu_\tau} = \phi^o_{\bar{\nu}_x} = \phi^o_{\bar{\nu}_\mu} = \phi^o_{\bar{\nu}_\tau}$. If the original fluxes were equal between flavors, any oscillation effect could be observed.

The survival probabilities can be written in terms of jump probabilities as [3]:

$$\begin{array}{l} P_{ee} = P_H P_L |U_{e1}|^2 + P_H(1 - P_L)|U_{e2}|^2 + (1 - P_H)|U_{e3}|^2 \\ \overline{P}_{ee} = (1 - \overline{P}_L)|U_{e1}|^2 + \overline{P}_L |U_{e2}|^2 \end{array} \tag{5}$$

for normal hierarchy ($\Delta m^2_{32} > 0$) and

$$\begin{array}{l} P_{ee} = P_L |U_{e1}|^2 + (1 - P_L)|U_{e2}|^2 \\ \overline{P}_{ee} = P_H(1 - \overline{P}_L)|U_{e1}|^2 + \overline{P}_L P_H |U_{e2}|^2 + (1 - P_H)|U_{e3}|^2 \end{array} \tag{6}$$

for inverted hierarchy ($\Delta m^2_{32} < 0$).

Considering the values of the jump probabilities and using the standard parametrization of the mixing matrix, the survival probabilities can be computed as shown in figure 2. The evolution of the probability P_{ee} ($\overline{P}_{ee}$) that a neutrino emitted as ν_e ($\bar{\nu}_e$) at the neutrinosphere remains as ν_e ($\bar{\nu}_e$) at Earth is plotted as a function of the θ_{13} mixing angle for different values of neutrino energy.

The upper plot corresponds to the normal hierarchy case (n.h.) and the lower one to the inverted hierarchy (i.h.). For n.h., the survival probability in the antineutrino channel does not depend on the neutrino energy and only very weakly on θ_{13}. However, the neutrino channel is very sensitive to θ_{13} via the P_H parameter. For inverted hierarchy the neutrino channel is independent on θ_{13} while the antineutrino channel depends on the 13-mixing angle and neutrino energy.

According to the adiabaticity conditions in the H resonance and the value of the θ_{13} angle, three regions can be distinguished. If energy spectra are different, then θ_{13} and the mass hierarchy can be probed as follows:

- For *small mixing angle* ($\sin^2\theta_{13} < 2 \times 10^{-6}$), there are no effects on θ_{13} and both hierarchies give similar results. Therefore, in this region we can not distinguish among hierarchies and only an upper bound on $\sin^2\theta_{13}$ can be set.

- For *intermediate* θ_{13} ($2 \times 10^{-6} < \sin^2\theta_{13} < 3 \times 10^{-4}$) maximal sensitivity to the angle is achieved and measurements of the angle are possible in this region.

[1] We neglect the possible effect of the propagation through the mass of the Earth.

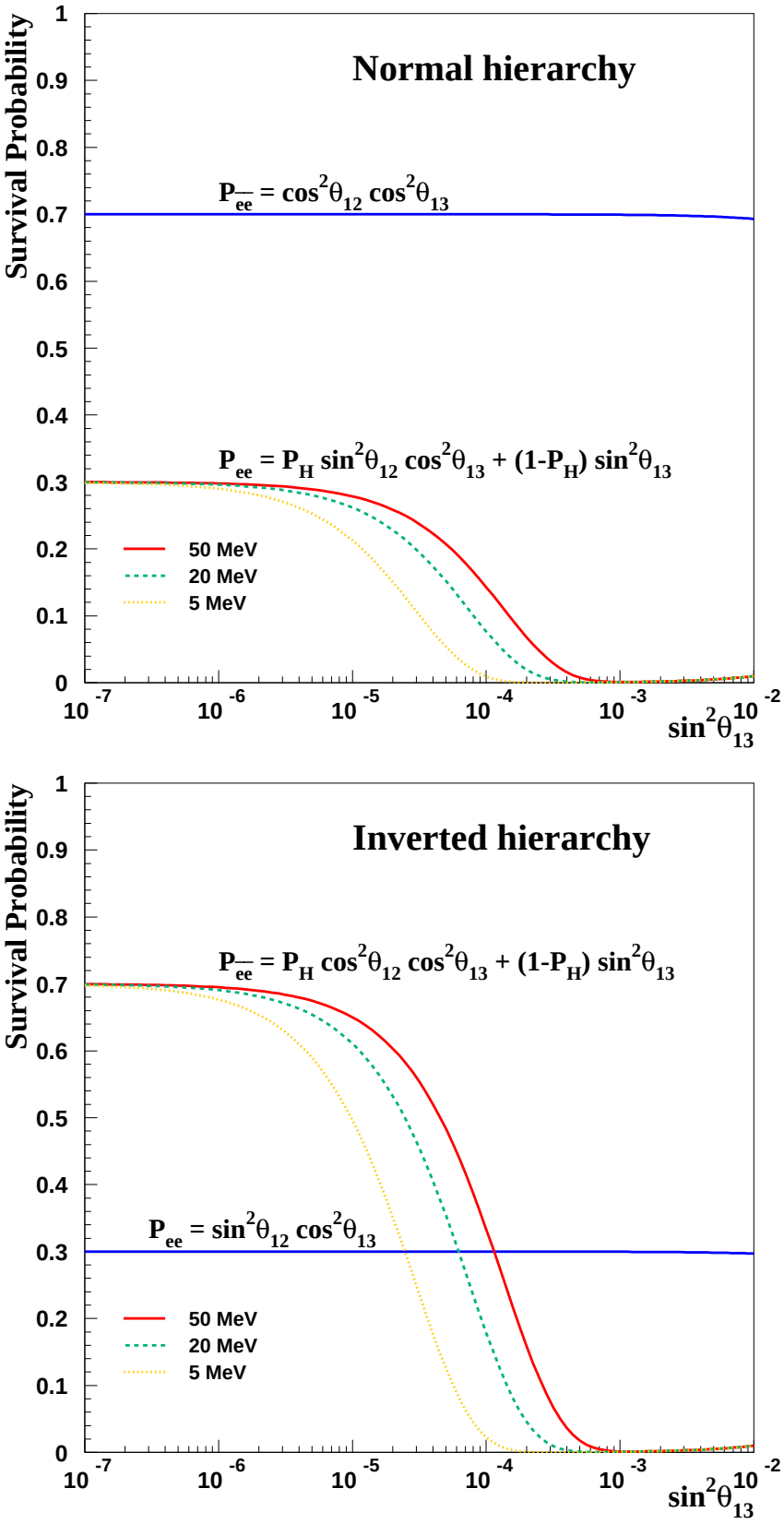

Figure 2: Survival probabilities for normal (top) and inverted (bottom) hierarchies as a function of $\sin^2\theta_{13}$ and different values of neutrino energies.

- For *large mixing angle* ($\sin^2\theta_{13} > 3\times10^{-4}$) maximal conversions occur. The effect of the mixing is strong in neutrino (antineutrino) channel if the mass hierarchy is normal (inverted). We are able to probe the mass hierarchy in this region but only a lower bound on θ_{13} can be put.

4 Cross-sections and expected supernova neutrino signal on liquid Ar detectors

At low energy, where nuclear processes dominate, three nuclei-scattering processes can be studied (ν_e charged current absorption on Ar with production of excited K, $\bar{\nu}_e$ charged current absorption on Ar with production of excited Cl and neutral current interactions on Ar from all neutrino flavors) in addition to elastic scattering on atomic electrons from all neutrino species. There is a possibility to separate the various channels by a classification of the associated photons from the K, Cl or Ar de-excitation, which exhibit specific spectral lines, or by the absence of associated photons in case of the elastic scattering.

In a liquid Argon TPC, it is hence possible to identify the following events:

1. **elastic scattering** on electrons

$$\overset{(-)}{\nu}\ e^- \rightarrow \overset{(-)}{\nu}\ e^- \tag{7}$$

2. **charged-current (CC) interactions on argon**

$$\nu_e\ {}^{40}Ar \rightarrow e^-\ {}^{40}K^* \tag{8}$$

$$\bar{\nu_e}\ {}^{40}Ar \rightarrow e^+\ {}^{40}Cl^* \tag{9}$$

3. **neutral-current (NC) interactions on argon**

$$\overset{(-)}{\nu}\ {}^{40}Ar \rightarrow \overset{(-)}{\nu}\ {}^{40}Ar^* \tag{10}$$

4.1 Elastic scattering processes

As well known, the elastic neutrino scattering off target-electrons has a total cross section that increases linearly with energy:

$$\begin{array}{lcll} \sigma(\nu_e e^- \rightarrow \nu_e e^-) & = & 9.20\times10^{-45} E_{\nu_e}(\mathrm{MeV}) & \mathrm{cm}^2 \\ \sigma(\bar{\nu}_e e^- \rightarrow \bar{\nu}_e e^-) & = & 3.83\times10^{-45} E_{\bar{\nu}_e}(\mathrm{MeV}) & \mathrm{cm}^2 \\ \sigma(\nu_{\mu,\tau} e^- \rightarrow \nu_{\mu,\tau} e^-) & = & 1.57\times10^{-45} E_{\nu_{\mu,\tau}}(\mathrm{MeV}) & \mathrm{cm}^2 \\ \sigma(\bar{\nu}_{\mu,\tau} e^- \rightarrow \bar{\nu}_{\mu,\tau} e^-) & = & 1.29\times10^{-45} E_{\bar{\nu}_{\mu,\tau}}(\mathrm{MeV}) & \mathrm{cm}^2 \end{array} \tag{11}$$

All neutrino species contribute to elastic scattering. The experimental signature consists in a single recoil electron. Since, the direction of this electron is highly correlated to the incoming ν direction, these events have the potentiality of precisely determining the location of the supernova source[19].

Figure 3 shows the cross sections of the elastic processes as a function of neutrino energy. We recall that the reaction involving ν_e's is the most probable since both CC and NC currents contribute. Electron antineutrinos are suppressed by helicity. The cross-section for muon and tau neutrinos is the smallest, since they proceed through NC current only.

These features are important since while the nature of the neutrino cannot be identified in elastic events, the total number of expected elastic events for a given flux depends on their nature because of its cross-section dependence. Hence, if the total flux of neutrino is constrained, the number of elastic events is sensitive to the nature of the neutrinos emitted by the supernova.

4.2 Nuclear processes

In order to compute the event rates, the relevant nuclear cross-sections must be in principle known with relatively good precision from energies ranging from a few MeV up to 100 MeV. For the nuclear processes, we use the calculations computed for the first time using the RPA including all the multipoles [20].

Figure 3 shows the cross sections of all the processes as a function of neutrino energy. The NC processes present high cross sections of the same order of magnitude as the ones from the CC reactions. They are even bigger than those from the $\bar{\nu}_e$CC events. This can be understood in terms of the energy threshold and nuclear effects of the various reactions. The Q–value of the ν_e CC is 1.50 MeV while for the $\bar{\nu}_e$ CC case is 7.48 MeV, hence electron antineutrinos are kinematically disfavored. In addition, the 1^+ and 0^+ allowed transitions are suppressed by nuclear structure reasons and the cross section is dominated by the other multipoles. Hence, electron antineutrinos cross-section is smaller than for neutrinos. The first excited state of Argon has an energy of 1.46 MeV with respect to the ground state, so the threshold for neutral current reaction is low.

In the case of the ν_e CC process, various estimates are available in the literature (see e.g. [21] and [22]). It was assumed in the past, that the $\nu_e{}^{40}Ar$ absorption rate proceeds through two main channels: the superallowed Fermi transition to the 4.38 MeV excited isobaric analog ^{40}K* state, and other Gamow-Teller transitions to several excited ^{40}K states. This assumption is correct for neutrino energies relevant to solar neutrino detection, however is not adequate for the energy range of supernova neutrinos, which extends up to 100 MeV. In the recent calculations that we use, the cross-section has been computed by random phase approximation (RPA) for neutrino energies up to 100 MeV, including all the multipoles up to J=6 and both parities. Figure 4 compares this cross section from three different sources: the dashed line corresponds to the shell model calculations performed by Ormand [21] considering only Fermi and Gamow–

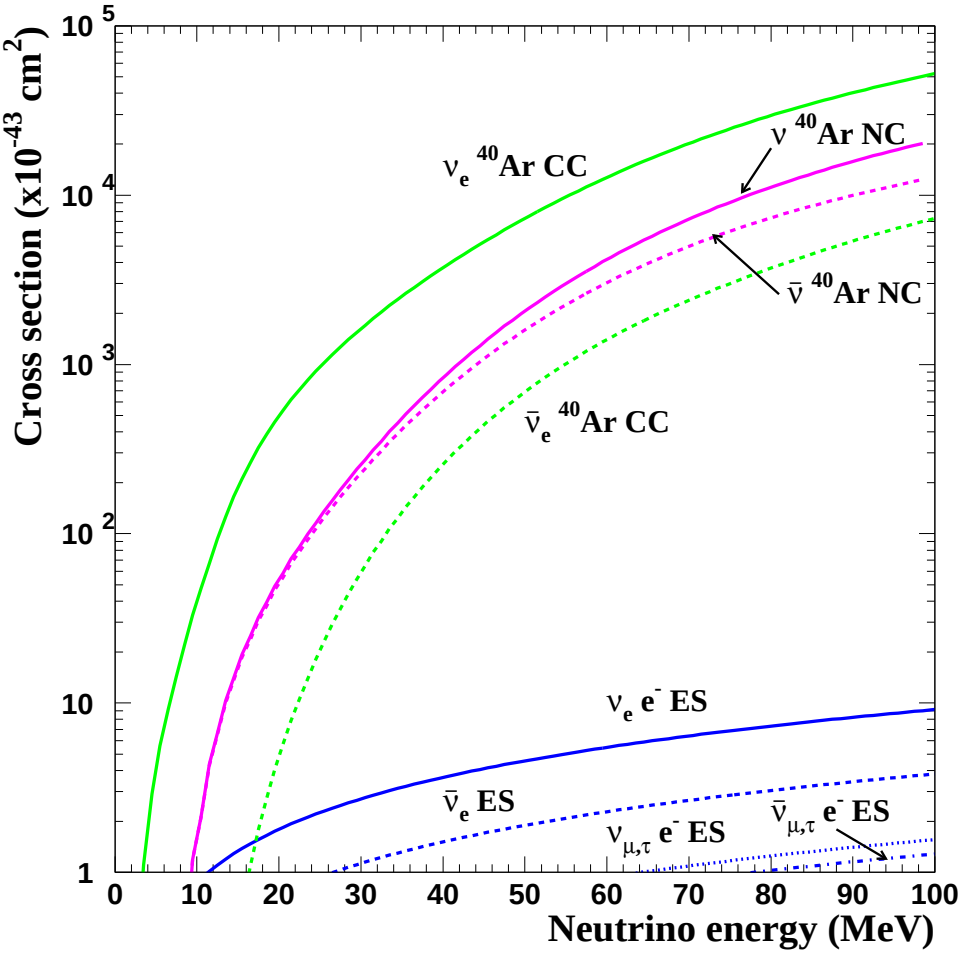

Figure 3: Neutrino cross sections relevant to the supernovae detection with a liquid Argon TPC detector.

Teller transitions; the dotted line is the assumption made in [16] where they take the total ν_e absorption cross section as 3 times the cross section of the pure Fermi transition computed in [22]; finally the solid line is the cross section used in this analysis [20].

We see that the assumption of $\sigma_{tot} = 3\,\sigma_F$ overestimates the cross section for energies smaller than 30 MeV, which is the energy range of ν_e from breakout, and therefore affects the expected number of events from the ν_e burst (discussed in section 5).

On the other hand, both Ormand and $\sigma_{tot} = 3\ \sigma_F$ cross sections underestimate the cross section for high energies up to 100 MeV, relevant for supernova neutrinos from the cooling phase (discussed in section 6). The cross section including all the multipoles grows faster than the others, showing that indeed not only the Fermi and Gamow–Teller transitions are important but also the rest of multipoles.

5 Supernova collapse and neutrino breakout phase

5.1 Time and energy dependence without neutrino oscillations

The neutrino shock breakout burst is the signal event in the supernova core collapse evolution. Its detection and characterization could test fundamental aspects of the current collapse supernova paradigm. The prompt electron neutrino burst is in principle observable and represents a diagnostic of the fundamental collapse supernova behavior. The characteristic time of the breakout burst is of the order of tens of ms.

The advantage of the early phase analysis is that it should not be affected by the time evolution of the density structure of the star nor whether the remnant is a neutron star or a black hole (see e.g. [16]). The shock wave takes about 2 seconds to reach the H-resonance region. Therefore, the potential time dependence of neutrino oscillations due to shock propagation can be neglected in this phase. Clean detection of the early part of the supernova signal is therefore a very important aspect of experimental supernova detection.

As already mentioned, a liquid Argon TPC has an excellent sensitivity to ν_e neutrinos mainly through the CC process. This provide unique information about the early breakout pulse. We will however show that neutral currents as well as elastic scattering, although lesser in rate, can provide important information as well on the shock breakout.

In order to study the detection of the shock breakout, we compute the differential number of neutrinos detected at a distance D from the supernova:

$$dN_{events} = \frac{N_{targets}}{4\pi D^2}\left(\frac{d^2N_\nu}{dE_\nu dt}\right)\sigma(E_\nu)dE_\nu dt \tag{12}$$

where $N_{targets}$ is the number of targets, D is the supernova distance, E_ν is the neutrino energy, t is the detector time, $dN_\nu/dE_\nu dt$ is the time and energy spectra of the neutrinos and $\sigma(E_\nu)$ is the cross section of a reaction process.

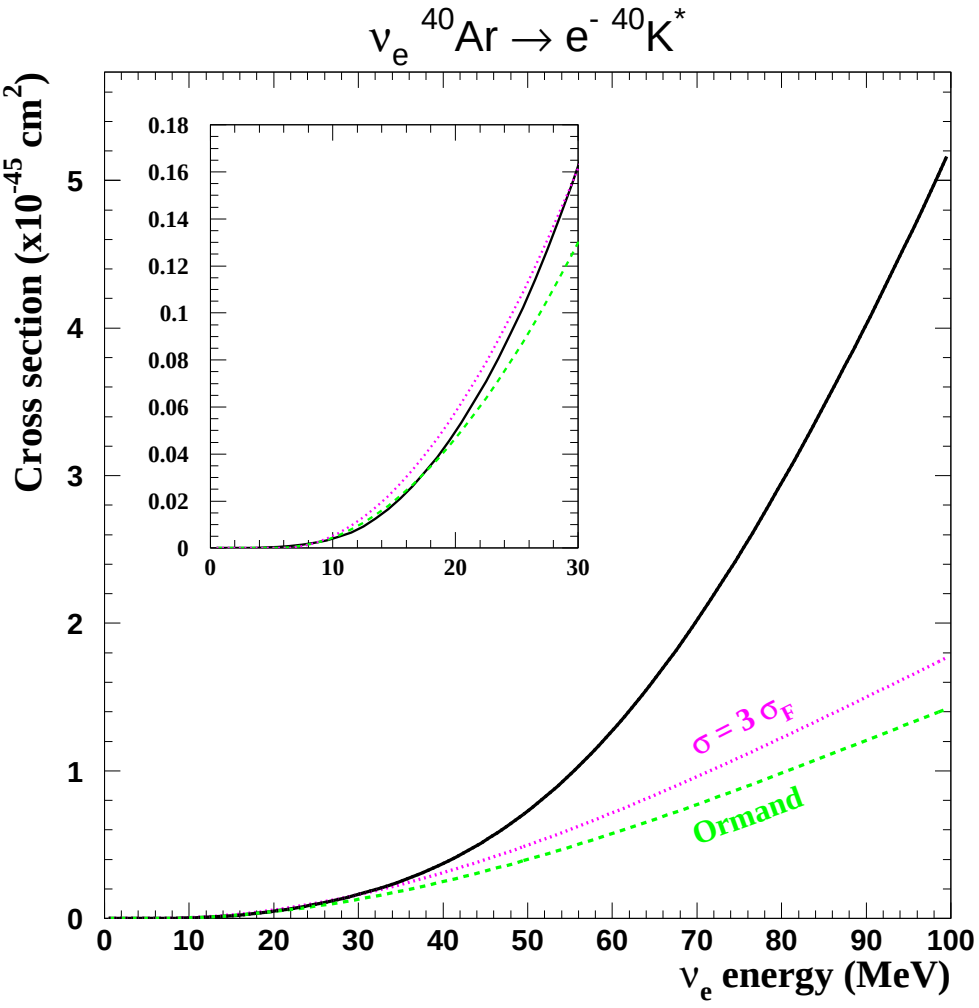

Figure 4: ν_e CC cross section as a function of the neutrino energy. The dashed line corresponds to the Ormand [21] cross section calculation, dotted line assumes that the total cross section of the absorption interaction is 3 times the cross section of the Fermi transition [16] and the solid line is the cross section used in this analysis calculated from RPA including all the transitions [20].

We use the simulation of the early phase of the neutrino burst performed by Burrows et al. [16] which yields $d^2N_\nu/dE_\nu dt$ in discrete steps of time.

The prediction for the time (energy integrated) evolution of the neutrino fluxes for the different flavors in absence of neutrino oscillations is shown in Figure 5(top). The time origin is defined such that the supernova core bounce time corresponds to $t = 200$ ms. This time is taken as the reference for the rest of the processes. The Figure 5 (bottom-left) shows the time–integrated energy spectrum of the first 470 ms of the time, namely up to 270 ms after the bounce. As expected, the flux is characterized by the bright peak of the ν_e emission due to the supernova shock breakout.

For comparison, we show in Figure 5(bottom-right) the particular energy distribution at 100 ms after the bounce ($t = 300$ ms). This picture illustrates how the energy spectra of the different neutrino flavors is predicted to change with time and how the bright ν_e becomes superseded by the neutrinos of all other flavors and helicities.

For the sake of calculations, we define the shock breakout burst by integrating up to $t = 240$ ms, namely we define a duration for the burst of 40 ms. We use these in the next section. In order to simplify the analysis, we treat the times after $t = 240$ ms as part of the cooling phase (see Section 6).

5.2 Effect of flavor oscillations and predicted event rates

Neutrino oscillations modify dramatically the flavor content of the neutrinos emitted from the supernova during the burst. A reduction of the ν_e peak due to the effect of oscillations can be readily understood from Figure 2, which plots the survival probability of electron neutrinos for normal and inverted mass hierarchies.

5.2.1 Small and large mixing angle approximations

We can first distinguish four limiting cases depending on the type of mass hierarchy and the value of the θ_{13} mixing angle (see equations 5 and 6 and Figure 2):

1. n.h.-L for normal mass hierarchy and large θ_{13}, where $P_{ee} \approx 0$ and $\overline{P}_{ee} \approx 0.7$,
2. n.h.-S for normal hierarchy and small θ_{13}, where $P_{ee} \approx 0.3$ and $\overline{P}_{ee} \approx 0.7$,
3. i.h.-L for inverted mass hierarchy and large θ_{13}, where $P_{ee} \approx 0.3$ and $\overline{P}_{ee} \approx 0$,
4. i.h.-S for inverted mass hierarchy and small θ_{13}, where $P_{ee} \approx 0.3$ and $\overline{P}_{ee} \approx 0.7$,

and where "small" (resp. "large") mean $\sin^2\theta_{13} < 2 \times 10^{-6}$ (resp. $\sin^2\theta_{13} > 3 \times 10^{-4}$). In the intermediate mixing angle region, there survival probability depends on the neutrino energy. Note that the no oscillation case corresponds to $P_{ee} \equiv 1$ and $\overline{P}_{ee} \equiv 1$.

We can therefore summarize the situation as follows: the suppression of the ν_e flavor is maximal in the case of a normal mass hierarchy and large θ_{13} mixing angle. This corresponds to the total conversion of ν_e's into $\nu_{\mu,\tau}$'s as they traverse the supernova

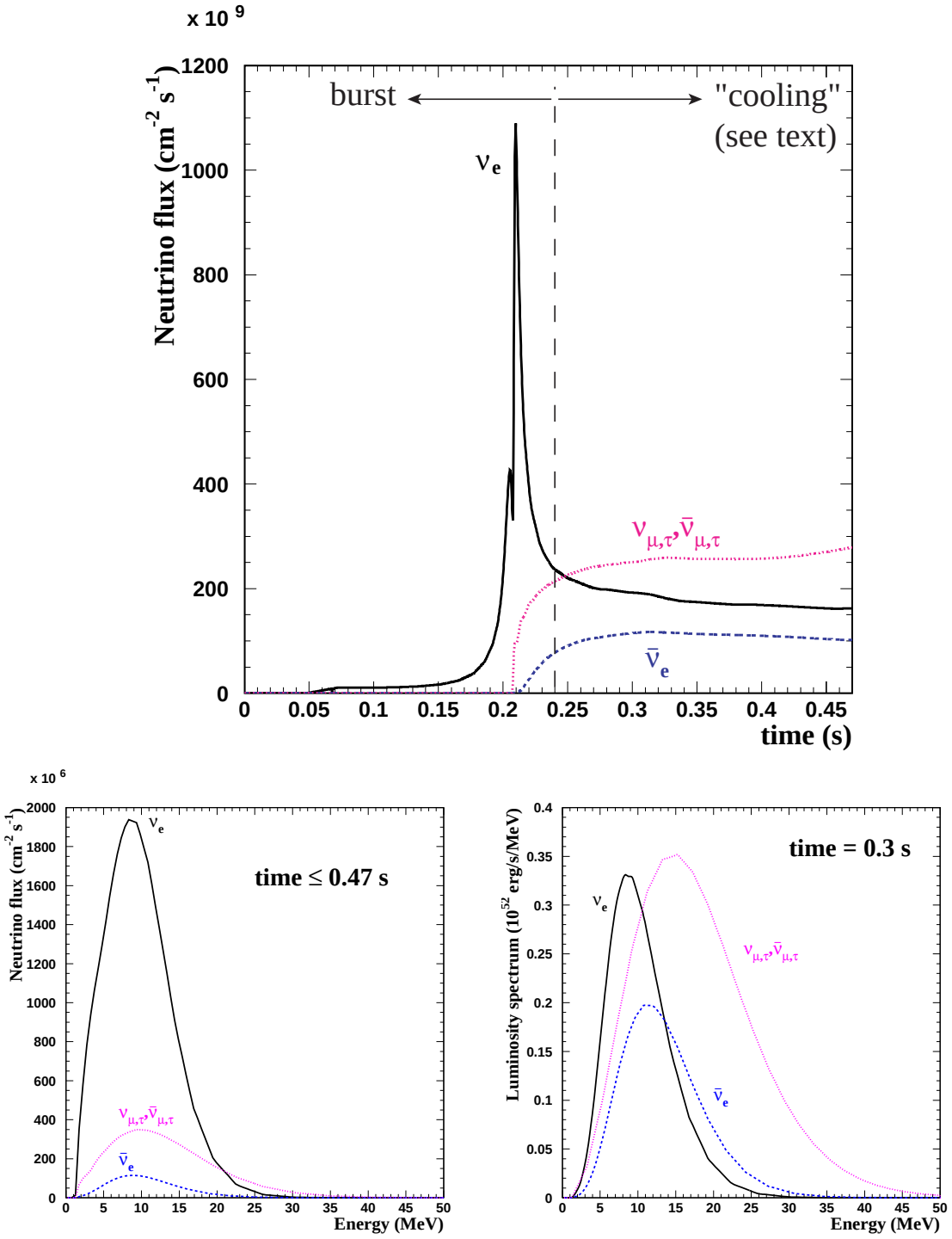

Figure 5: Illustration of the prediction of [16] without neutrino flavor oscillations: prediction of the neutrino flux at Earth at a distance of 10 kpc (top), time–integrated energy spectrum corresponding to the first 270 ms after the bounce (bottom-left) and luminosity spectrum of ν_e (solid line), $\bar{\nu}_e$ (dashed line) and $\nu_{\mu,\tau}$, $\bar{\nu}_{\mu,\tau}$ (dotted line) neutrinos at 100 ms after the shock breakout (bottom-right). We treat the times before t=240 ms as "burst" and after as "cooling".

Reaction		Burst (t < 240 ms) – 3 kton detector				
		No oscillation	Oscillation (n.h.) Large θ_{13}	Oscillation (n.h.) Small θ_{13}	Oscillation (i.h.) Large θ_{13}	Oscillation (i.h.) Small θ_{13}
Elastic						
	$\nu_e\, e^-$	2	<1	1	1	1
	$\bar{\nu}_e\, e^-$	<1	<1	<1	<1	<1
	$(\nu_\mu + \nu_\tau)\, e^-$	<1	<1	<1	<1	<1
	$(\bar{\nu}_\mu + \bar{\nu}_\tau)\, e^-$	<1	<1	<1	<1	<1
	total $\nu\, e^-$	2	<1	1	1	1
Absorption						
CC	ν_e ^{40}Ar	8	2	4	4	4
	$\bar{\nu}_e$ ^{40}Ar	<1	<1	<1	<1	<1
NC	ν ^{40}Ar	1	1	1	1	1
	$\bar{\nu}$ ^{40}Ar	<1	<1	<1	<1	<1
Total		11	3	6	6	6

Table 2: Expected neutrino events in a 3 kton detector during the burst (see text for definition). Neutrino oscillations with matter effects are included for different mass hierarchies and θ_{13} values.

matter. For the other cases, the oscillation reduces the expected ν_e flux by a factor 3 compared to the non-oscillation case.

Tables 2 and 3 show the expected number of events during the burst in a 3 kton and 70 kton liquid Argon TPC detector, respectively, for the four oscillation scenarios and compares them to the non oscillation case. For completeness we have separated the contributions from ν_e's, $\nu_{\mu,\tau}$'s and similarly for antineutrinos. However, it should be recalled that four channels are in fact accessible experimentally: the ν_e CC, the $\bar{\nu}_e$ CC, the NC and the elastic scattering.

With the assumed distance of 10 kpc, the burst produces in a 3 kton detector and in absence of neutrino oscillations 2 elastic events, 8 ν_e CC and 1 NC event for a total of 11 events. In case of the 70 kton detector, the rates are 37 elastic events, 192 ν_e CC and 39 NC event for a total of 268 events.

We consider first the elastic events. As already mentioned, oscillation has a strong effect on the ν_e burst. The ν_e will be suppressed by a factor 3 for three of the four oscillation scenarios we have considered, or can even be maximally suppressed in the case of normal mass hierarchy and large θ_{13}. Neutrino flavor oscillation is of course a unitary process, hence, the oscillated ν_e's will be transformed into other flavors. However, since the cross-section for the elastic ν_e process is higher than for other processes, we expect a reduction of the number of elastic events. Indeed, as visible in Tables 2 and 3, the elastic burst signal is highly suppressed for the oscillation scenarios. With our definition of burst, with the assumption of a 40 ms duration, there is in fact a smaller component of ν_μ's, ν_τ's, $\bar{\nu}_\mu$'s, $\bar{\nu}_\tau$'s and $\bar{\nu}_e$'s (see Figure 5). Finally, the elastic events are suppressed by a factor roughly 4 for the case of a normal mass hierarchy and large θ_{13} mixing angle, and roughly by a factor 2 for the other cases.

Reaction		Burst (t < 240 ms) – 70 kton detector				
		No oscillation	Oscillation (n.h.) Large θ_{13}	Oscillation (n.h.) Small θ_{13}	Oscillation (i.h.) Large θ_{13}	Oscillation (i.h.) Small θ_{13}
Elastic						
	$\nu_e\, e^-$	34	3	12	12	12
	$\bar{\nu}_e\, e^-$	1	1	1	1	1
	$(\nu_\mu + \nu_\tau)\, e^-$	1	6	5	5	5
	$(\bar{\nu}_\mu + \bar{\nu}_\tau)\, e^-$	1	1	1	1	1
	total $\nu\, e^-$	37	11	19	19	19
Absorption						
CC	ν_e ^{40}Ar	192	41	86	86	86
	$\bar{\nu}_e$ ^{40}Ar	<1	<1	<1	1	<1
NC	ν ^{40}Ar	28	28	28	28	28
	$\bar{\nu}$ ^{40}Ar	11	11	11	11	11
Total		268	91	144	145	144

Table 3: Expected neutrino events in a 70 kton detector during the burst (see text for definition). Neutrino oscillations with matter effects are included for different mass hierarchies and θ_{13} values.

We now turn to the nuclear charged current events. The ν_e CC reaction is in principle a golden channel to study the burst. Because of the oscillation of ν_e into other flavors (not completely compensated by oscillation of other flavors into ν_e), the size of the peak is reduced compared to the non-oscillation case: the suppression is almost a factor 5 for the case of a normal mass hierarchy and large θ_{13} mixing angle, and roughly a factor 2.5 for the other cases.

Finally, we can consider the neutral current events. Obviously they are not affected by oscillations, since neutral currents are flavor symmetric. They hence constitute an excellent probe for the supernova properties independent of the neutrino oscillation intrinsic properties. We therefore stress the importance of this signal to decouple supernova from oscillation physics. Unfortunately the rates in the 3 kton detector are rather modest: at the level of one event (independent of the oscillation scenario). For the case of a 70 kton detector, we expect in total 39 events (independent of the oscillation scenario).

The information about the shock breakout mechanism that can be extracted from the 3 kton detector is hence marginal, in particular in the case of the reduced number of expected events because of oscillation effects. A supernova could explode at a closer distance, however, this is an unlikely event. In contrast, a 70 kton detector could provide hundreds of events, enough statistics to study the ν_e neutrinos from the burst.

5.2.2 Study of energy spectra

The importance of the statistics can be appreciated when one studies the energy spectra of the events. Sufficient statistics would allow to study the energy spectra of the events

which provides an extra signature to separate supernova from oscillation physics.

Figures 6–9 contain the time evolution of the expected events in the burst for the different detection channels, namely ν_e CC, $\bar{\nu}_e$ CC, elastic and neutral currents, normalized to 70 kton detector and the corresponding time integrated event spectra. The non oscillation and the four different oscillation cases are compared in the plots. For the ν_e CC, $\bar{\nu}_e$ CC and elastic events we also show the event energy distributions. For the neutral current events, the energy cannot be determined due to the neutrino in the final state.

The reduction of the ν_e peak due to the effect of oscillations can be seen in figure 6. The suppression is maximal for normal hierarchy and large θ_{13} mixing angle due to the total conversion of ν_e into $\nu_{\mu,\tau}$. At the same time, the energy spectrum moves slightly to higher neutrino energy values.

Elastic events (figure 8) are also sensitive to the oscillations with a reduction of the shock breakout peak. However, the energy spectrum remains almost unchanged.

The neutral current events (figure 9) are not affected by neutrino oscillations and the time evolution clearly shows the shock breakout peak coming from ν_e events.

Overall, we note that the energy distribution of the burst is marginally affected by oscillations.

5.2.3 Consequence of the neutrino burst detection

We can hence conclude that the burst signal is only affected in rate by the effect of neutrino oscillation and the effect on the shape is marginal. This means that:

- a clear SN burst peak should be visible in the neutral current sample, regardless of the neutrino oscillation physics. This signature should provide a clear indication for the nature of the supernova explosion. The size of the peak determines the burst absolute neutrino flux from the supernova.

- the oscillation physics occurring during the early phase of the supernova can be studied by detection of the ν_e and $\bar{\nu}_e$ CC channels.

- the number of observed ν_e CC observed in the burst can distinguish between the non oscillation case, the n.h.-L oscillation and the three other oscillation scenarios. The n.h.-S, i.h.-L and i.h.-S cases cannot be distinguished by ν_e CC.

- a roughly factor 4 enhancement of observed $\bar{\nu}_e$ CC observed in the burst would be a clear indication for an oscillation matter enhancement only possible in the inverted mass hierarchy with large mixing angle. Otherwise, a roughly factor 2 enhancement is expected from the effect of oscillations (see Figure 7). It should be stressed that this effect is not visible even for a 70 kton detector.

- elastic events can help distinguish between the non oscillation case, the n.h.-L oscillation case and the three other oscillation scenario.

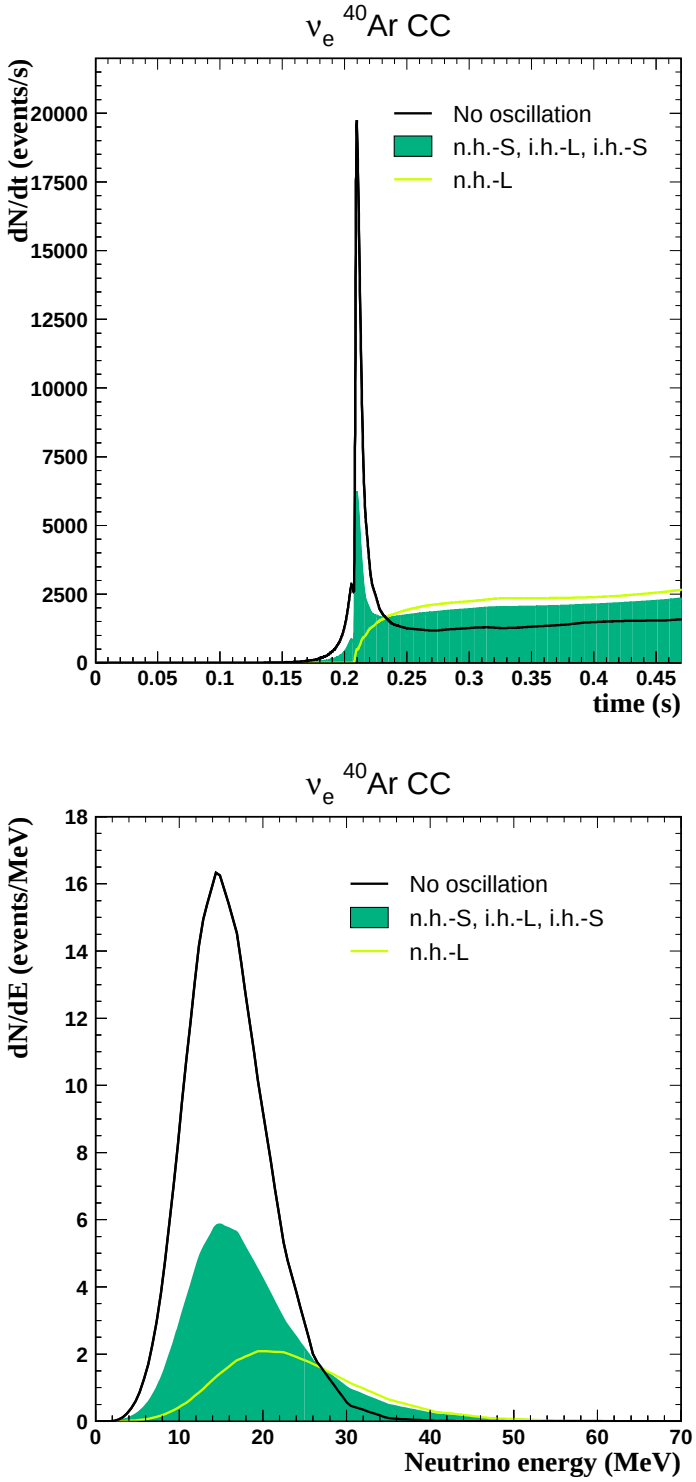

Figure 6: SN burst: time evolution of the ν_e CC event rate (top) and the corresponding time integrated event spectra (bottom). The non oscillation (dark curve), n.h.–L (light curve) and n.h.–S, i.h.–L and i.h.–S (dark region) cases are considered.

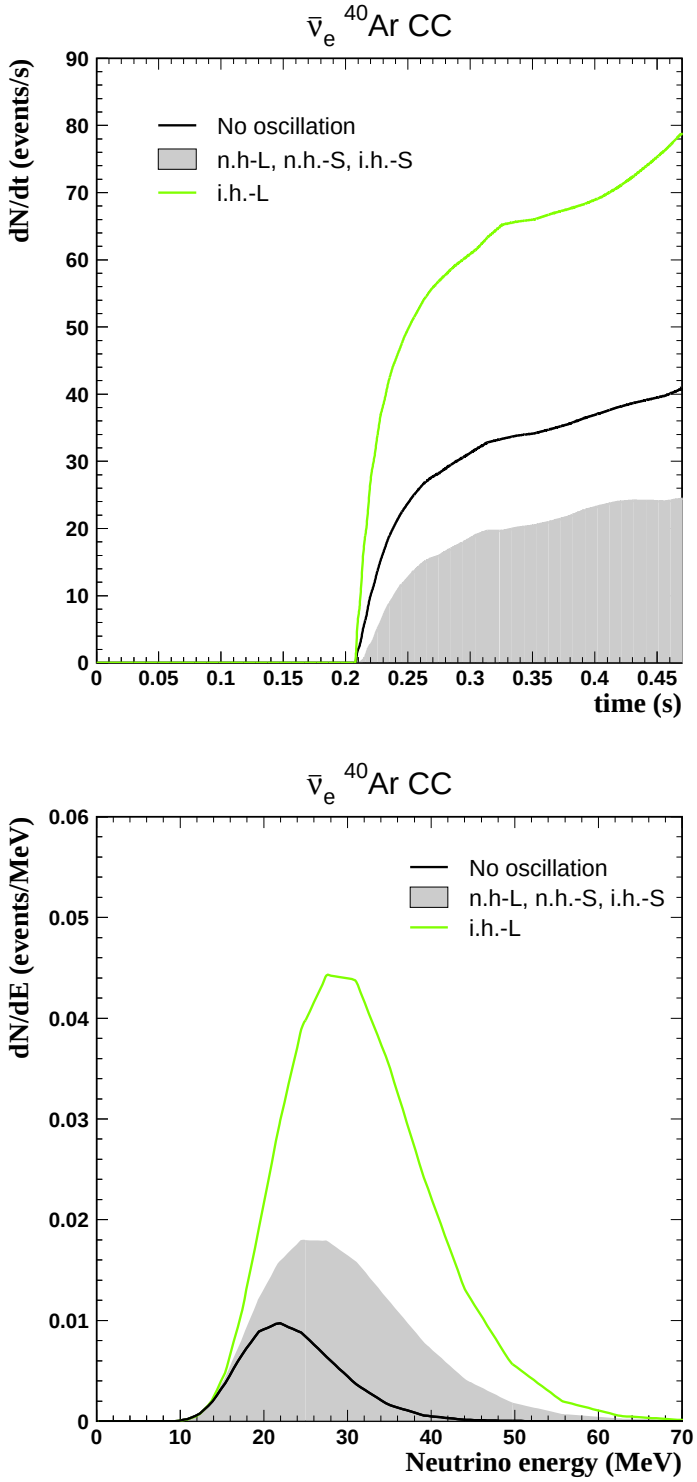

Figure 7: SN burst: time evolution of the $\bar{\nu}_e$ CC event rate (top) and the corresponding time integrated event spectra (bottom). The non oscillation (dark curve), i.h.–L (light curve) and n.h.–L, n.h.–S and i.h.–S (gray region) cases are considered.

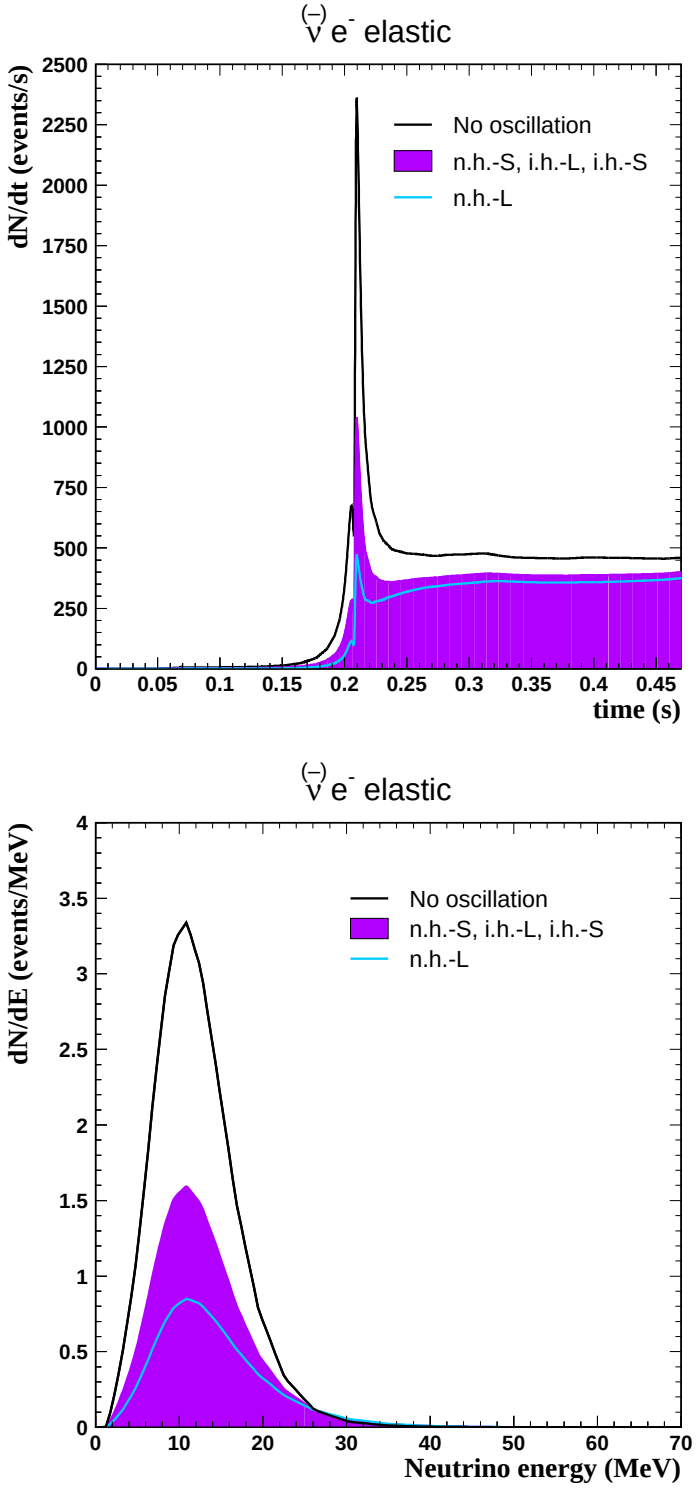

Figure 8: SN burst: time evolution of the elastic event rate (top) and the corresponding time integrated event spectra (bottom). The non oscillation (dark curve), n.h.–L (light curve) and n.h.–S, i.h.–L and i.h.–S (dark region) cases are considered.

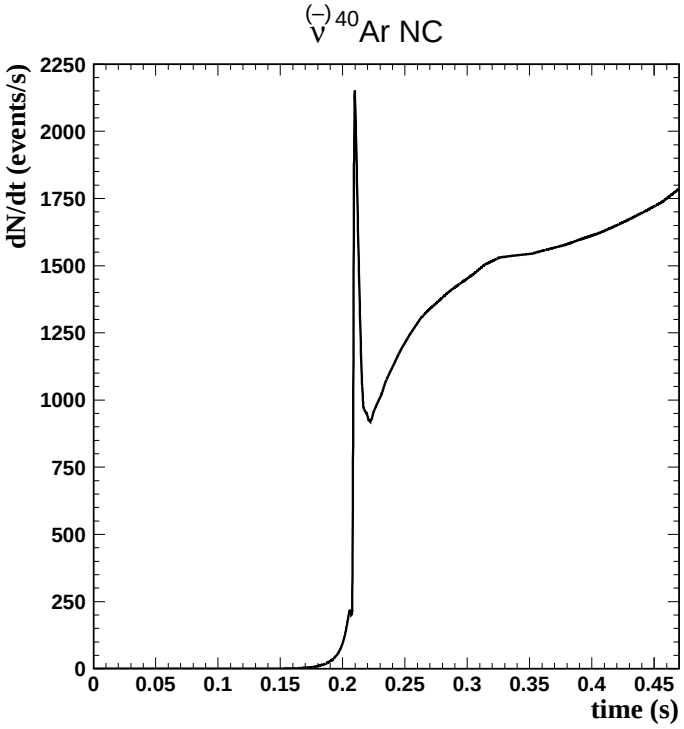

Figure 9: SN burst: time evolution of the NC event rate.

5.2.4 General mixing case – intermediate mixing angle

For the intermediate mixing angle region defined approximately by $\approx 10^{-5} < \sin^2\theta_{13} < 2 \times 10^{-4}$, the number of expected events varies strongly with the mixing angle. In fact, in this region, we expect that the neutrino oscillation effect depends on the neutrino energy within the range up to 100 MeV relevant for supernova neutrinos.

The actual variation of the number of events as a function of the θ_{13} value are summarized in Figure 10 for the four detection channels. Solid lines correspond to the normal mass hierarchy case, dotted lines to the inverted mass hierarchy case and dashed lines to the non oscillation case. We consider events in burst and the plots are normalized to a 70 kton detector.

This variation can be exploited to measure the mixing angle if it lies in this intermediate region. Quantitative estimate of the precision with which the angle can be determined will be described elsewhere [23].

5.3 Comparison with other experiments

All experiments will be affected in the same way by the effect of neutrino flavor oscillation in their expected rates of ν_e events. In order to compare experiments, we hence restrict ourself to the case where neutrino oscillations are neglected and compare rates in Superkamiokande and SNO with our results on Argon. Results can be readily scaled

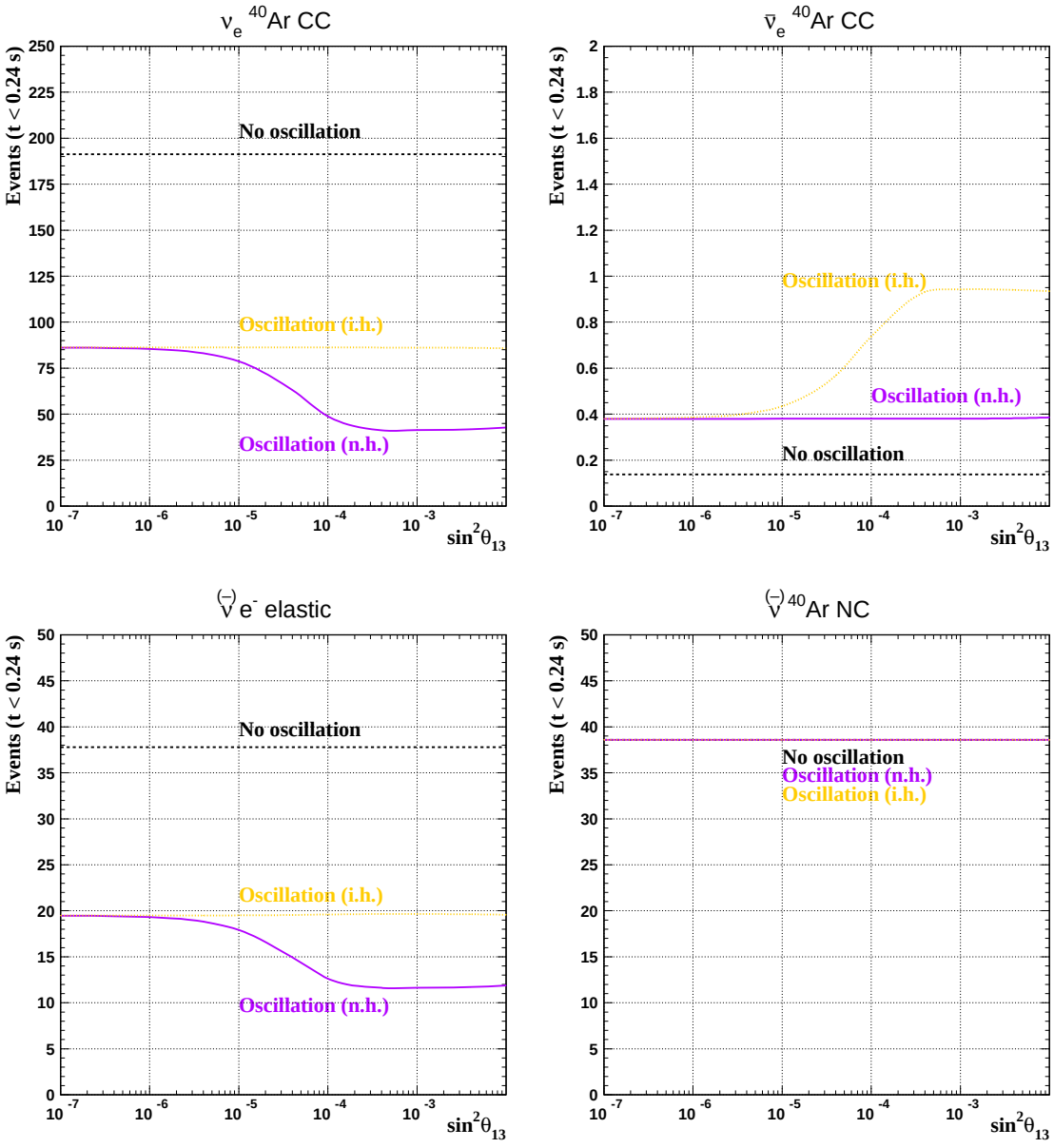

Figure 10: Expected number of events in a 70 kton detector during the burst (see text for definition) as a function of $\sin^2\theta_{13}$. The different neutrino interaction processes are plotted separately. Solid lines correspond to the n.h. oscillation case, dotted lines to the i.h. case and dashed lines to the non oscillation case.

to include neutrino oscillation effects.

The integrated number of ν_e events as a function of time for elastic and absorption processes without including oscillation effects are plotted in figure 11. The main contribution comes from the CC channel. Figure 12 shows for comparison similar plots for SuperKamiokande (SK) and SNO detectors.

The SK volume for supernova neutrino detection is 32 kton of light water. The dominant reaction is the charged–current absorption of $\bar{\nu}_e$ neutrinos on free protons ($\bar{\nu}_e p \rightarrow n e^+$). Neutrino scattering on electrons ($\nu e^- \rightarrow \nu e^-$) also contributes for all neutrino species. For the study of the shock breakout we calculate the event rates in SK due to only the ν_e elastic scattering. For this process we use the neutrino electron scattering cross section given in [24] with a threshold of ~ 5 MeV. If there is large mixing angle between ν_e and ν_μ or ν_τ neutrinos, the early ν_e signal will be reduced significantly in SK.

The SNO detector is a light and heavy water neutrino detector containing 1 kton of D_2O surrounded by a cavity of 1.6 kton of light water. The main reactions for ν_e neutrinos are the elastic scattering and the NC and CC reactions on deuterium ($\nu_e d \rightarrow np\nu_e$ and $\nu_e d \rightarrow ppe^-$). The cross sections used to compute these events are taken from [25].

Figure 13 shows the comparison between the expected number of events from the ν_e burst in the three experiments. A total of 10 events are expected in the 3kton ICARUS in the 40 ms after the bounce: 8 events from the absorption channel and 2 from the elastic channel. The contribution of SK and SNO for the same interval of time is 20 and 7 events, respectively.

Summarizing, we observe that the event statistics that would be obtained in SuperKamiokande, SNO and the 3 kton ICARUS are similar. In this case, SNO and ICARUS benefit largely from their direct sensitivity to ν_e via charged current interactions on resp. deuteron and Argon, while in SuperKamiokande one has to rely on elastic scattering on electrons, which has a much smaller cross-section. Hence, smaller detectors like SNO and ICARUS can compare favorably with the largest SuperKamiokande in the study of the breakout phase.

We also conclude that given that neutrino oscillations is an established fact [2], it will be difficult to study the neutrino burst within the current round of experiments given the reduction of statistics following the conversion of ν_e into other flavors. In the context of the liquid Argon TPC, it appears that a 70 kton detector will be mandatory in order to collect sufficient events to study the neutrino burst.

6 Cooling phase

In this section we will refer to the main neutrino emission phase in the core collapse supernovae: the cool-off of the star.

As seen in previous sections, the energy spectra of the expected neutrinos at the

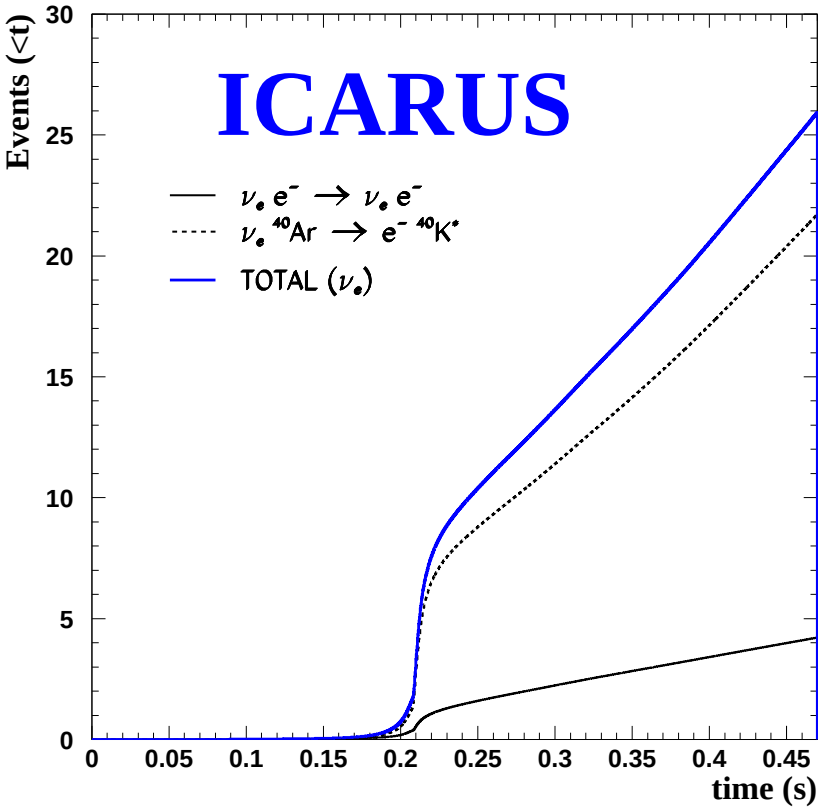

Figure 11: Integrated number of ν_e events as a function of time for the elastic and absorption channels. The thick solid line corresponds to the total number of events for a 3 kton detector. No oscillation effects are included.

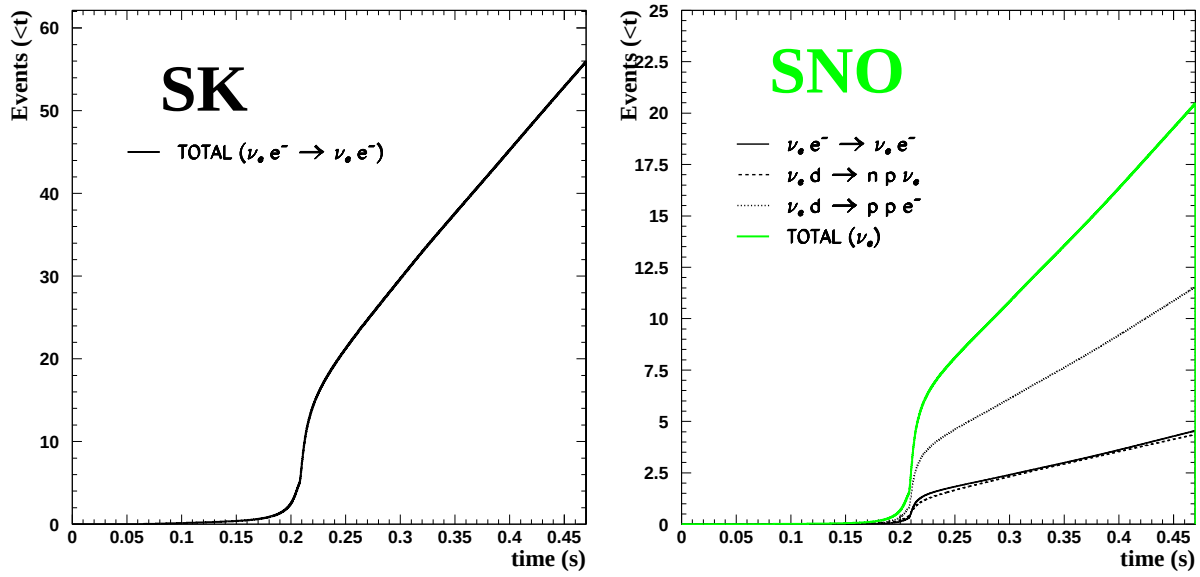

Figure 12: Integrated number of ν_e events as a function of time expected in the SK (left) and SNO (right) detectors. No oscillation effects are included.

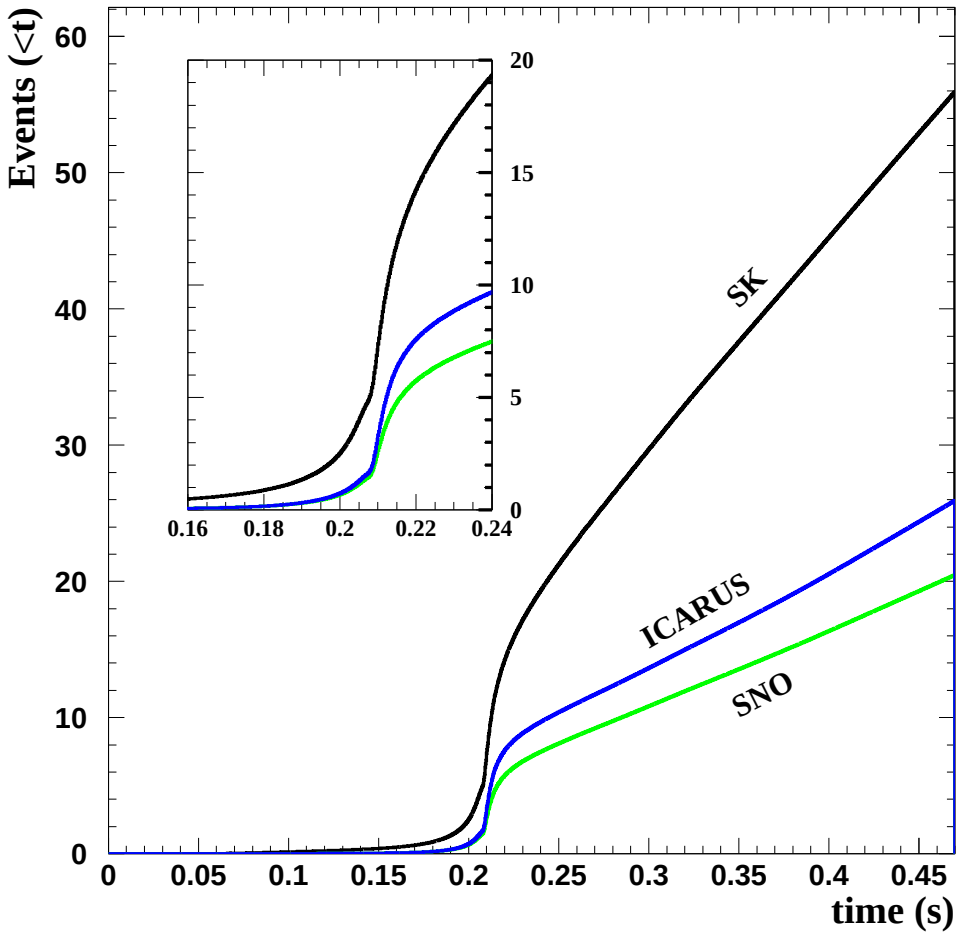

Figure 13: Comparison of the expected number of events from the ν_e breakout burst in a 3 kton ICARUS, SK and SNO experiments. In the first 40 ms after bounce a total of 20 events are expected in SK, 10 in ICARUS and 7 in SNO. No oscillation effects are included.

detector is modified by oscillations among flavors since the average neutrino energies are flavor dependent and the interaction cross sections are different for different flavors. The variations of the neutrino energy will depend on the adiabaticity conditions on the H and L resonances in the supernova and on the neutrino oscillation parameters. Four different cases are considered in this analysis depending on the type of mass hierarchy and the value of the θ_{13} mixing angle.

6.1 Hierarchical energy distribution – scenario I

We first consider the prediction from Ref [17] which we parameterize as Fermi-Dirac distributions with $\langle E_{\nu_e} \rangle = 11$ MeV, $\langle E_{\bar{\nu}_e} \rangle = 16$ MeV, $\langle E_{\nu_{\mu,\tau}} \rangle = \langle E_{\bar{\nu}_{\mu,\tau}} \rangle = 25$ MeV and luminosity equipartition among flavors. In this kind of scenario where the energies are rather different (hierarchical) between flavors, the effect of the oscillation is the most pronounced. Indeed, oscillations will as expected harden the ν_e spectrum, which has a big incidence of the ν_e CC channel.

Table 4 contains the number of neutrino events from a supernova at 10 kpc expected in the 3 kton detector. Elastic, CC and NC processes have been considered independently and oscillation and non oscillation cases have been computed for normal and inverted hierarchies. However, we recall that four channels are in fact accessible experimentally: the ν_e CC, the $\bar{\nu}_e$ CC, the NC and the elastic scattering.

We note that:

- the number of observed ν_e CC observed can distinguish between (a) the non oscillation case, (b) the n.h.-L case and (c) the three other oscillation scenarios. n.h.-S, i.h.-L and i.h.-S cannot be distinguished by ν_e CC.
- a roughly factor 4 enhancement of observed $\bar{\nu}_e$ CC observed would be a clear indication for an oscillation matter enhancement only possible in the inverted mass hierarchy with large mixing angle. Otherwise, a roughly factor 2 enhancement is expected from the effect of oscillations.

As was mentioned in section 3, normal and inverted hierarchies are degenerated for small θ_{13} in all the cases. In the neutrino (antineutrino) channel and i.h. (n.h.) the conversion is adiabatic and results are independent on θ_{13}. Maximal conversion occurs for large mixing angle in the neutrino (antineutrino) channel for n.h. (i.h.).

We stress again that the ν_e flux and $\bar{\nu}_e$ flux have different information about the neutrino oscillation parameters. The i.h.-L and i.h.-S are distinguishable from $\bar{\nu}_e$ events but are not from ν_e events. Then, a good separation of these events is important in order to distinguish between models.

Figures 14, 15 and 16 show these effects in the neutrino energy spectra. The plots on the top correspond to the expected number of neutrinos arriving at Earth and the bottom plots are the corresponding number of events detected in a 3 kton detector. The four oscillation cases are considered in the distributions.

Reaction		Scenario I				
		No oscillation	Oscillation (n.h.) Large θ_{13}	Oscillation (n.h.) Small θ_{13}	Oscillation (i.h.) Large θ_{13}	Oscillation (i.h.) Small θ_{13}
Elastic						
	$\nu_e\, e^-$	20	20	20	20	20
	$\bar{\nu}_e\, e^-$	8	8	8	8	8
	$(\nu_\mu + \nu_\tau)\, e^-$	7	7	7	7	7
	$(\bar{\nu}_\mu + \bar{\nu}_\tau)\, e^-$	6	6	6	6	6
	total $\nu\, e^-$	41	41	41	41	41
Absorption						
CC	ν_e ^{40}Ar	188	962	730	730	730
	$\bar{\nu}_e$ ^{40}Ar	15	33	33	75	33
NC	ν ^{40}Ar	492	492	492	492	492
	$\bar{\nu}$ ^{40}Ar	419	419	419	419	419
Total		1155	1947	1715	1757	1715

Table 4: Expected neutrino events in a 3 kton detector including neutrino oscillations with matter effects inside the supernova. The flux parameters are $\langle E_{\nu_e} \rangle = 11$ MeV, $\langle E_{\bar{\nu}_e} \rangle = 16$ MeV, $\langle E_{\nu_{\mu,\tau}} \rangle = \langle E_{\bar{\nu}_{\mu,\tau}} \rangle = 25$ MeV and luminosity equipartition among flavors is assumed.

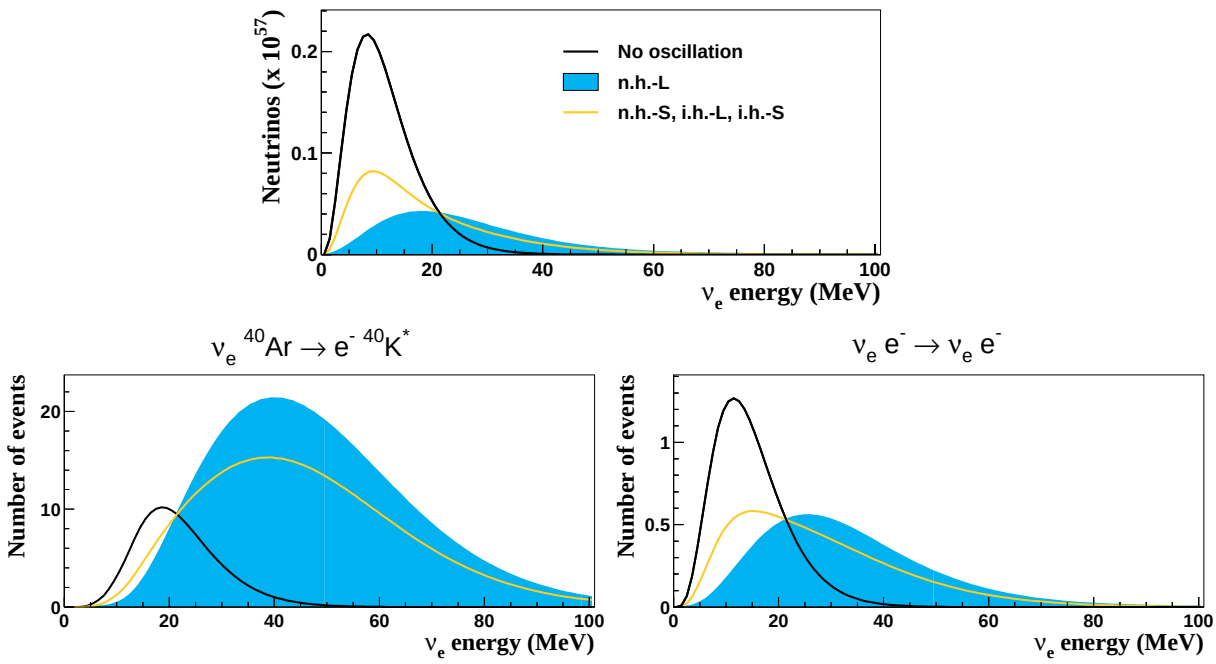

Figure 14: Scenario I: Number of ν_e neutrinos arriving at Earth (top) and expected number of events in the 3 kton detector (bottom) for ν_e neutrinos. The non oscillation and the four oscillation cases have been taken into account. The CC interaction process (left) and elastic scattering (right) are split in the figure.

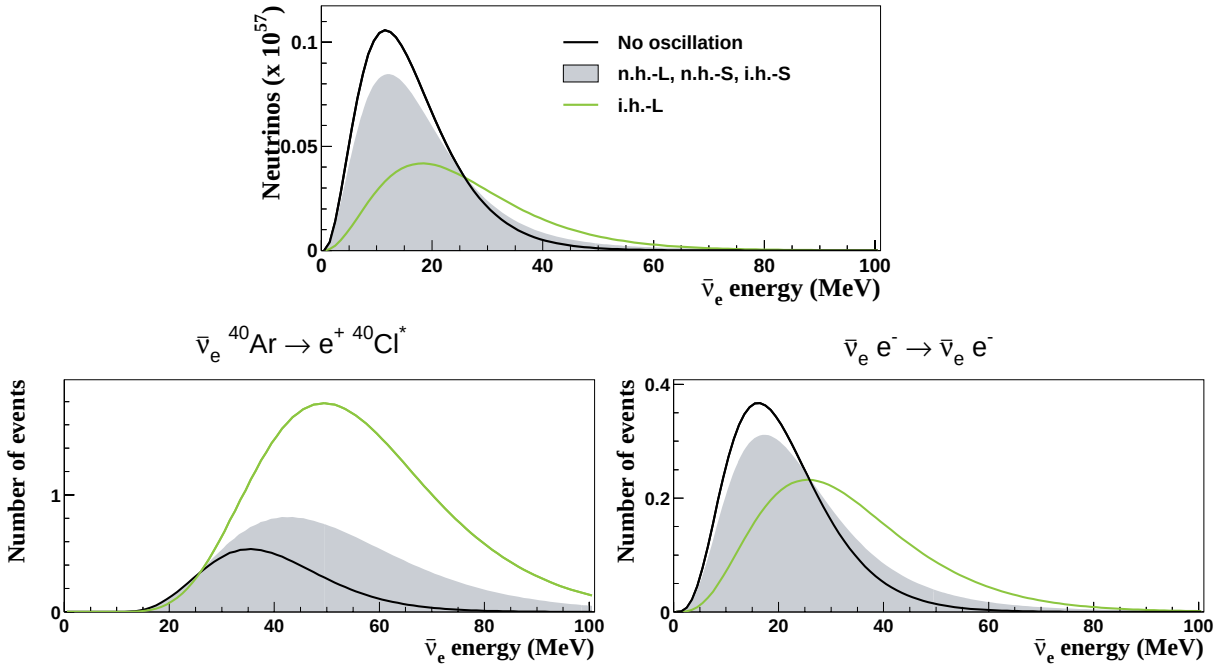

Figure 15: Scenario I: Number of $\bar{\nu}_e$ neutrinos arriving at Earth (top) and expected number of events in the 3 kton detector (bottom) for $\bar{\nu}_e$ neutrinos. The non oscillation and the four oscillation cases have been taken into account. The CC interaction process (left) and elastic scattering (right) are split in the figure.

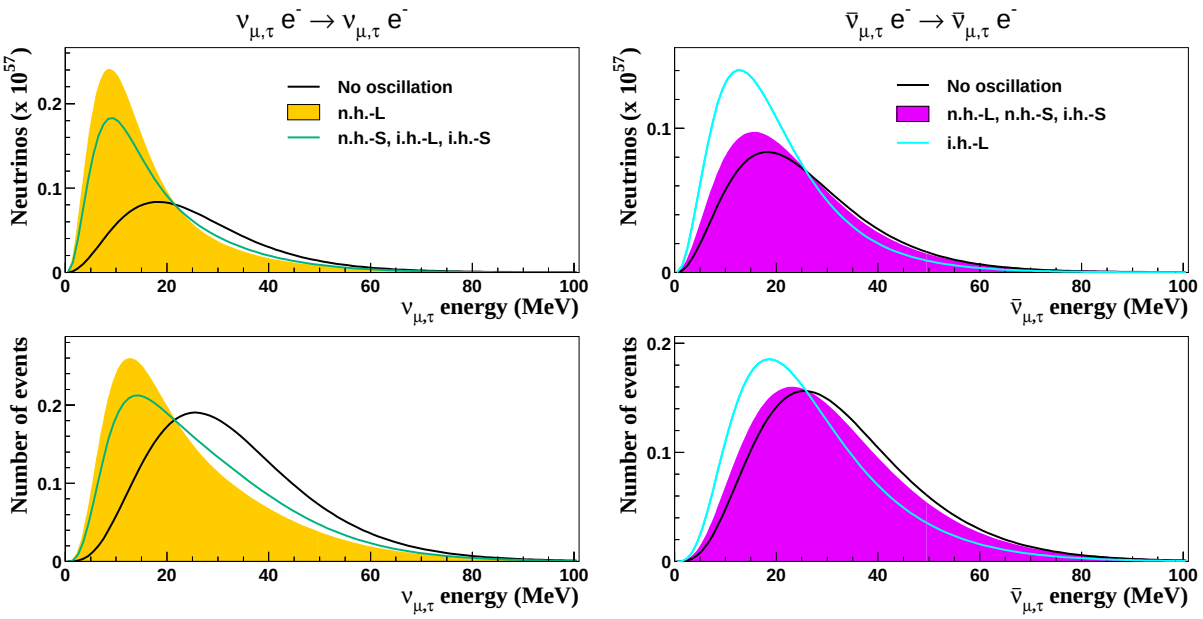

Figure 16: Scenario I: Number of neutrinos arriving at Earth (top) and expected number of events in the 3 kton detector (bottom) for $\nu_{\mu,\tau}$ (left) and $\bar{\nu}_{\mu,\tau}$ (right) neutrinos. The non oscillation and the four oscillation cases have been taken into account.

Due to the total conversion $\nu_{\mu,\tau} \rightarrow \nu_e$ for the n.h.-L case, the ν_e energy spectra is harder and this leads a huge increase of the expected events due to the quadratic dependence of the CC cross section with energy. The same effect can be seen for $\bar{\nu}_e$ events and i.h.-L case. The elastic processes are less sensitive to the oscillations and smaller number of events is expected. Nevertheless, the energy spectrum is modified specially for $\nu_{\mu,\tau}$ events, moving to lower values of energy due to the neutrino mixing.

6.1.1 General results as a function of the mixing angle

The explicit variation of the expected rates and energy spectra with the θ_{13} angle can be computed considering the dependence of the jump probability with this angle (section 3).

Figure 17 shows the the variation of the neutrino rates as a function of $\sin^2\theta_{13}$. We compare the expected results for the cases of n.h. (solid line), i.h. (dotted line) and no oscillation (dashed line). CC events are very sensitive to the change on the energy spectra due to oscillations. A clear increase on the number of events is expected, being of a factor (4–5) for ν_e CC events and a factor 2 for $\bar{\nu}_e$ CC interactions. The main variations with the angle θ_{13} are expected for the ν_e CC channel in the case of normal hierarchy and for the $\bar{\nu}_e$ CC channel for inverted hierarchy. The number of ν_e CC events increases 30% from small to large θ_{13} values and $\bar{\nu}_e$ CC events are doubled. Small variations are expected for the rest of channels.

Although the number of events does not change for some reactions, the energy spectra are affected by oscillations and in particular by the value of the θ_{13} angle.

6.2 Other cooling scenarios – scenarios II–V

The signature of neutrino oscillations depends on the flavor-dependent primary supernova neutrino fluxes. Recent SN simulations [7, 18] found that the differences between the average energies of $\nu_{\mu,\tau}$, $\bar{\nu}_{\mu,\tau}$ and $\bar{\nu}_e$ are in the range 0–20%, with 10% being a typical number. The luminosities of all neutrino flavors are expected to be approximately equal within a factor two.

In order to consider the range of possibilities for the source fluxes we compute the expected events for different values of the neutrino average energies and luminosities, as summarized in table 1. The results from the different scenarios are contained in tables 5–8. Table 5 is obtained using the flux parameters found by the Livermore group [10].

In table 6 we take the results from [7, 18] and equipartition luminosities. Finally, tables 7 and 8 show the expected rates considering the same average energies than used in table 6 but for two extreme cases of luminosity partition: $L_{\nu_e} = L_{\bar{\nu}_e} = 2\ L_{\nu_x}$ (table 7) and $L_{\nu_e} = L_{\bar{\nu}_e} = 0.5\ L_{\nu_x}$ (table 8), with ν_x each of ν_μ, ν_τ, $\bar{\nu}_\mu$ and $\bar{\nu}_\tau$ neutrino flavors.

Clearly, scenarios III–V distinguish themselves from the scenarios I–II in their prediction of a quite flavor degenerate spectra (see figures 14, 15 and 16). In order to illustrate this, we show in Figure 18 how these affect the neutrino energy spectra. The

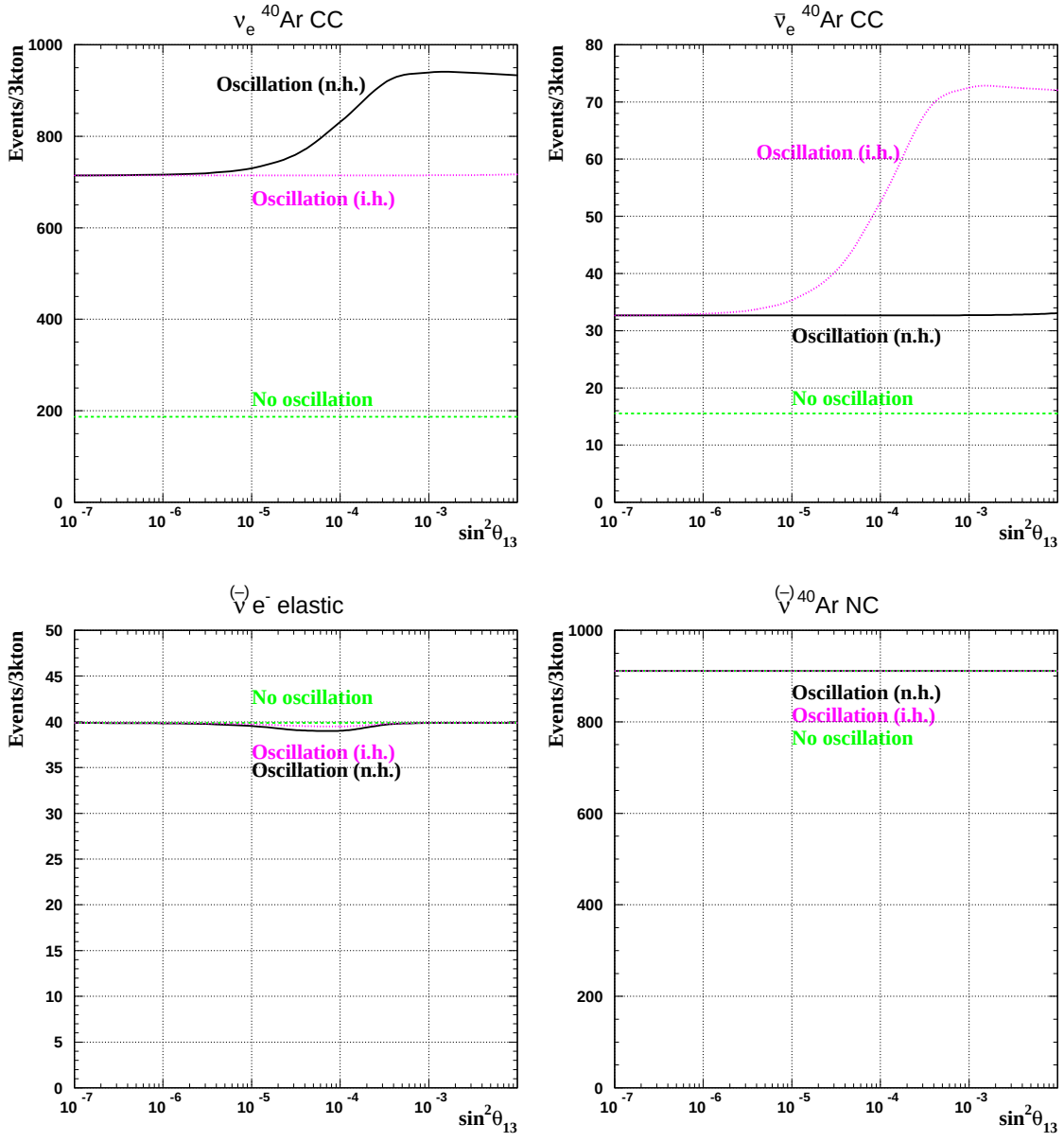

Figure 17: Expected number of events in a 3 kton detector as a function of $\sin^2\theta_{13}$. The different neutrino interaction processes expected are plotted separately. Solid lines correspond to the n.h. oscillation case, dotted lines to the i.h. case and dashed lines to the non oscillation case.

Reaction		Scenario II				
		No oscillation	Oscillation (n.h.) Large θ_{13}	Oscillation (n.h.) Small θ_{13}	Oscillation (i.h.) Large θ_{13}	Oscillation (i.h.) Small θ_{13}
Elastic						
	$\nu_e\, e^-$	20	20	20	20	20
	$\bar{\nu}_e\, e^-$	8	8	8	8	8
	$(\nu_\mu + \nu_\tau)\, e^-$	7	7	7	7	7
	$(\bar{\nu}_\mu + \bar{\nu}_\tau)\, e^-$	5	5	5	5	5
	total $\nu\, e^-$	40	40	40	40	40
Absorption						
CC	ν_e ^{40}Ar	264	805	644	644	644
	$\bar{\nu}_e$ ^{40}Ar	16	28	28	57	28
NC	ν ^{40}Ar	415	415	415	415	415
	$\bar{\nu}$ ^{40}Ar	355	355	355	355	355
Total		1090	1643	1482	1511	1482

Table 5: Expected neutrino events in a 3 kton detector. The flux parameters are $\langle E_{\nu_e} \rangle$ = 13 MeV, $\langle E_{\bar{\nu}_e} \rangle = 16$ MeV, $\langle E_{\nu_{\mu,\tau}} \rangle = \langle E_{\bar{\nu}_{\mu,\tau}} \rangle = 23$ MeV and luminosity equipartition among flavors is assumed.

upper plot corresponds to the expected number of neutrinos arriving at Earth and the bottom plot is the event energy spectrum normalized to a 3 kton detector. The three scenarios III–V are considered in the distributions, each time for the non oscillation and for the oscillation case with a normal mass hierarchy and large mixing angle.

6.3 Discrimination between the various scenarios

The comparison between the different scenarios is summarized in figure 19. The expected number of events in the four neutrino detection channels are plotted for the five scenarios of the SN neutrino flux parameters considered in this study. Moreover, the non oscillation and the four oscillation cases are plotted for every scenario. The plots are normalized to a supernova at 10 kpc and a 3 kton detector. The errors indicated in the picture correspond to statistical errors and give a visual feeling on the ability to separate the various supernova (I–V) and oscillation scenarios (no osc, n.h.-L, n.h.-S, i.h.-L, i.h.-S).

NC events are sensitive to the primary source parameters and are independent to the oscillation effects. They give a direct account for the total luminosity of the supernova and of the hardness of the neutrino spectra. Hence, they provide the means to discriminate between the various supernova physics scenarios if the binding energy is assumed to be known. This is illustrated in the bottom plot of Figure 19. The rates of the nuclear processes are such that excellent statistical precision is achieved. They amount to 911 ± 30, 770 ± 27, 422 ± 20, 387 ± 20, 450 ± 21 events for resp. the scenarios I–V, where the error quoted is the statistical error on the number of events.

Reaction		Scenario III				
		No oscillation	Oscillation (n.h.) Large θ_{13}	Oscillation (n.h.) Small θ_{13}	Oscillation (i.h.) Large θ_{13}	Oscillation (i.h.) Small θ_{13}
Elastic						
	$\nu_e\, e^-$	20	20	20	20	20
	$\bar{\nu}_e\, e^-$	8	8	8	8	8
	$(\nu_\mu + \nu_\tau)\, e^-$	7	7	7	7	7
	$(\bar{\nu}_\mu + \bar{\nu}_\tau)\, e^-$	5	5	5	5	5
	total $\nu\, e^-$	40	40	40	40	40
Absorption						
CC	ν_e ^{40}Ar	264	482	417	417	417
	$\bar{\nu}_e$ ^{40}Ar	16	18	18	23	18
NC	ν ^{40}Ar	215	215	215	215	215
	$\bar{\nu}$ ^{40}Ar	207	207	207	207	207
Total		742	962	897	902	897

Table 6: Expected neutrino events in a 3 kton detector. The flux parameters are $\langle E_{\nu_e} \rangle$ = 13 MeV, $\langle E_{\bar{\nu}_e} \rangle = 16$ MeV, $\langle E_{\nu_{\mu,\tau}} \rangle = \langle E_{\bar{\nu}_{\mu,\tau}} \rangle = 17.6$ MeV and luminosity equipartition among flavors is assumed.

Reaction		Scenario IV				
		No oscillation	Oscillation (n.h.) Large θ_{13}	Oscillation (n.h.) Small θ_{13}	Oscillation (i.h.) Large θ_{13}	Oscillation (i.h.) Small θ_{13}
Elastic						
	$\nu_e\, e^-$	29	15	19	19	19
	$\bar{\nu}_e\, e^-$	12	10	10	6	10
	$(\nu_\mu + \nu_\tau)\, e^-$	5	8	7	7	7
	$(\bar{\nu}_\mu + \bar{\nu}_\tau)\, e^-$	4	5	5	6	5
	total $\nu\, e^-$	50	38	41	38	41
Absorption						
CC	ν_e ^{40}Ar	397	362	372	372	372
	$\bar{\nu}_e$ ^{40}Ar	24	22	22	17	22
NC	ν ^{40}Ar	188	188	188	188	188
	$\bar{\nu}$ ^{40}Ar	199	199	199	199	199
Total		858	809	822	814	822

Table 7: Expected neutrino events in a 3 kton detector. The flux parameters are $\langle E_{\nu_e} \rangle$ = 13 MeV, $\langle E_{\bar{\nu}_e} \rangle = 16$ MeV, $\langle E_{\nu_{\mu,\tau}} \rangle = \langle E_{\bar{\nu}_{\mu,\tau}} \rangle = 17.6$ MeV and luminosities $L_{\nu_e} = L_{\bar{\nu}_e} = 2\ L_{\nu_x}$ with ν_x each of ν_μ, ν_τ, $\bar{\nu}_\mu$ and $\bar{\nu}_\tau$ neutrino flavors are considered.

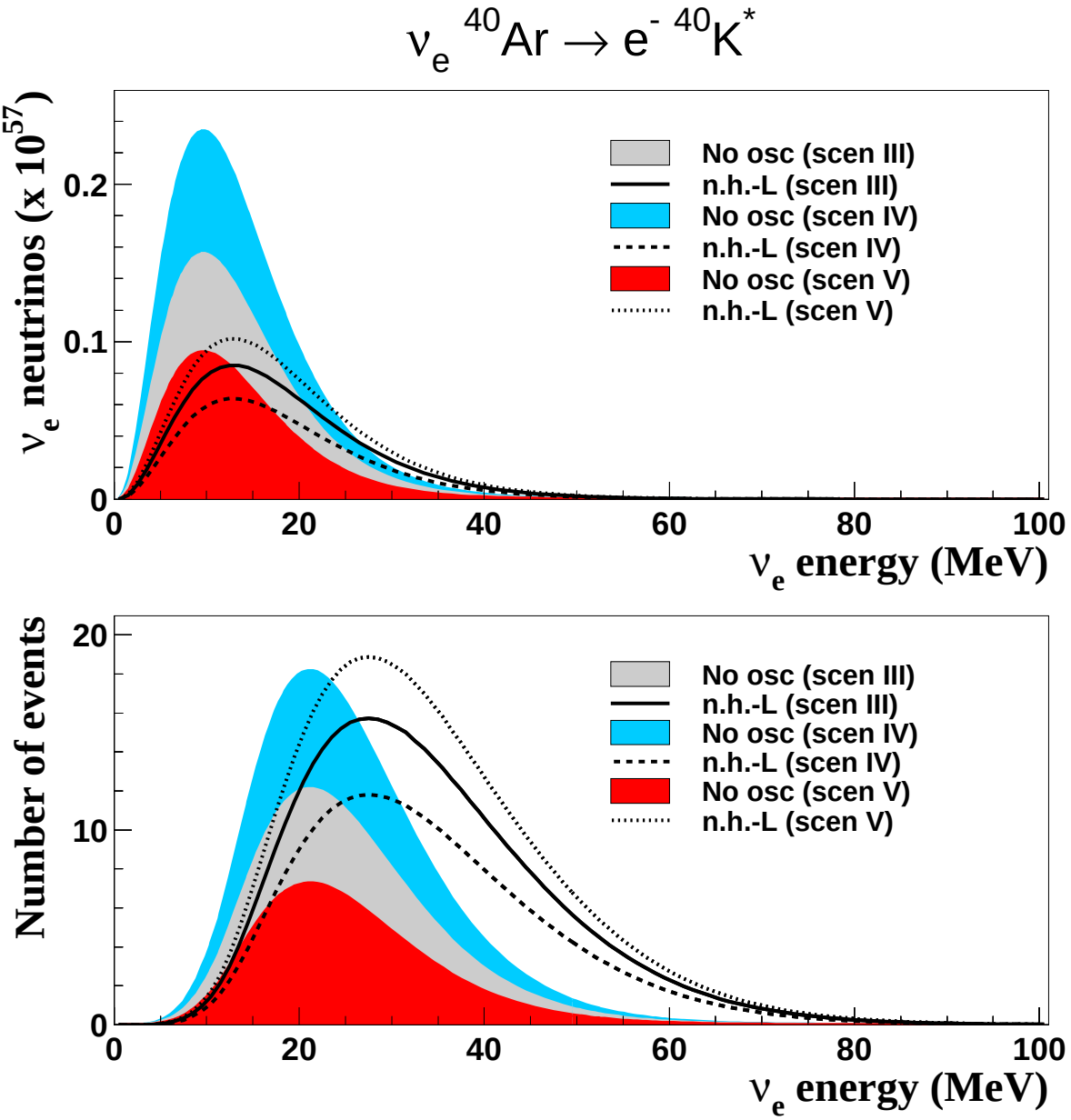

Figure 18: Scenarios III–V: number of ν_e neutrinos arriving at Earth (top) and expected number of events in the 3 kton detector (bottom) for ν_e neutrinos. The three scenarios III–V are considered in the distributions, each time for the non oscillation and n.h.-L oscillation cases.

Reaction		Scenario V				
		No oscillation	Oscillation (n.h.) Large θ_{13}	Oscillation (n.h.) Small θ_{13}	Oscillation (i.h.) Large θ_{13}	Oscillation (i.h.) Small θ_{13}
Elastic						
	$\nu_e\, e^-$	12	23	20	20	20
	$\bar{\nu}_e\, e^-$	5	6	6	10	6
	$(\nu_\mu + \nu_\tau)\, e^-$	8	6	7	7	7
	$(\bar{\nu}_\mu + \bar{\nu}_\tau)\, e^-$	7	6	6	5	6
	total $\nu\, e^-$	32	41	39	42	39
Absorption						
CC	ν_e ^{40}Ar	159	578	453	453	453
	$\bar{\nu}_e$ ^{40}Ar	10	15	15	28	15
NC	ν ^{40}Ar	236	236	236	236	236
	$\bar{\nu}$ ^{40}Ar	214	214	214	214	214
Total		651	1084	957	973	957

Table 8: Expected neutrino events in a 3 kton detector. The flux parameters are $\langle E_{\nu_e} \rangle$ = 13 MeV, $\langle E_{\bar{\nu}_e} \rangle$ = 16 MeV, $\langle E_{\nu_{\mu,\tau}} \rangle = \langle E_{\bar{\nu}_{\mu,\tau}} \rangle$ = 17.6 MeV and luminosities $L_{\nu_e} = L_{\bar{\nu}_e}$ = 0.5 L_{ν_x} with ν_x each of ν_μ, ν_τ, $\bar{\nu}_\mu$ and $\bar{\nu}_\tau$ neutrino flavors are considered.

The supernova and neutrino oscillation physics can then be studied by the simultaneous observation of NC, ν_e CC, $\bar{\nu}_e$ CC and elastic channels. We observe:

- In the hierarchical scenarios (I–II) the enhancement of ν_e due to oscillation is highly significant. As already mentioned, this is the result of the hardening of the spectrum in all cases of oscillations.
  - The effect is of course the strongest in the case of n.h.-L for the ν_e and in the case of i.h.-L for $\bar{\nu}_e$.
  - The normal and inverted hierarchy yield the same number of events in the case of small mixing.
- In the non-hierarchical scenarios (III–V) the enhancement of ν_e due to oscillation is significant compared to the non-oscillation case, except for scenario (IV) where the quasi-degenerate energies and the choice of luminosities $L_{\nu_e} = L_{\bar{\nu}_e} = 2\ L_{\nu_x}$ with ν_x each of ν_μ, ν_τ, $\bar{\nu}_\mu$ and $\bar{\nu}_\tau$ neutrino flavors just washes out the oscillation (the disappearing $\nu_e \to \nu_x$ are compensated by the appearing $\nu_x \to \nu_e$).
- in the scenario IV this ambiguity in the number of events can be solved by a study of the event energy distribution (see Figure 18). Indeed, the figure clearly shows that the spectrum is indeed harder for the oscillation case but that the total number of events is roughly the same.

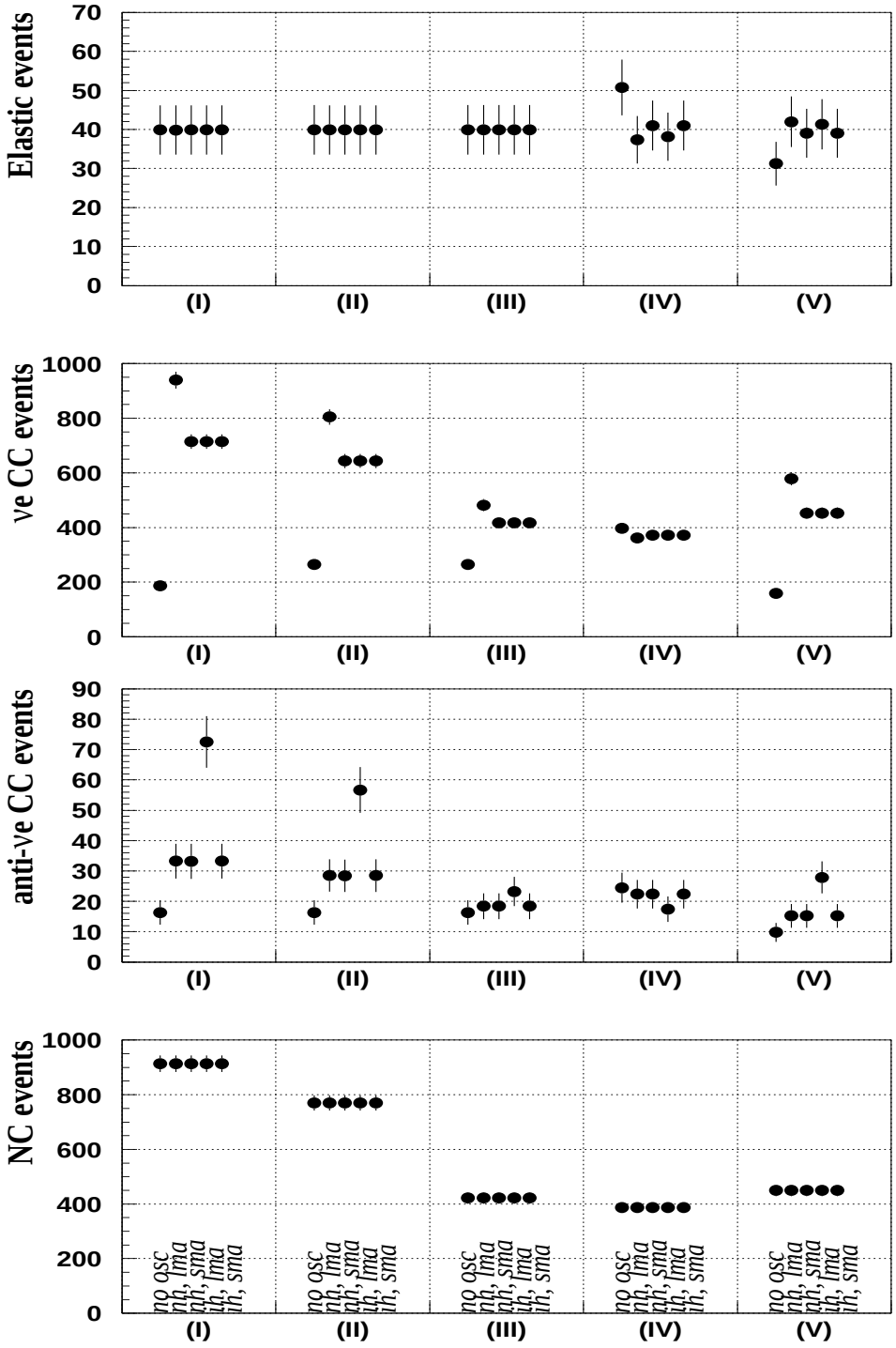

Figure 19: Expected number of events: the four neutrino processes are considered for different SN scenarios and oscillation conditions (see text). The statistical errors are included in the picture.

7 Conclusions

An analysis of the neutrino events expected in a liquid Argon TPC (ICARUS-like) from a future galactic supernova has been performed showing the high capabilities of the detector to observe neutrinos from stellar collapses and extract information about their properties.

Four detection channels have been considered: elastic scattering on atomic electrons from all neutrino species, ν_e charged current absorption on Ar with production of excited K, $\bar{\nu}_e$ charged current absorption on Ar with production of excited Cl and neutral current interactions on Ar from all neutrino flavors.

We give a detailed account of the dependence with the mixing angle θ_{13} and the type of mass hierarchy. Neutrino oscillations change significantly the expected supernova neutrino rates and energy spectra. The matter effects inside the supernova must be included to predict how the spectra of the neutrino burst is modified by oscillations.

Information about the supernova explosion mechanism can be obtained from the study of the neutrino burst. The early phase neutrino signal on Argon has been computed using the fluxes from a realistic core collapse supernova model [16], and including oscillation effects. Thanks to its clean identification and high sensitivity to ν_e neutrinos, a liquid Argon TPC can provide fundamental information about the shock breakout mechanism. We find that a 70 kton detector is best suited to study the SN burst, given its statistics even in case of the ν_e suppression expected in case of oscillations.

For the cooling phase of the supernova, we have adopted a simple Fermi-Dirac parameterization of the neutrino fluxes. We selected six different scenarios in order to take into account the uncertainties on the knowledge of the supernova physics and estimate their effect on our analysis. For the study of the cooling phase, a 3 kton detector is sufficient to collect hundreds of events which could provide fundamental information on supernova and neutrino oscillation physics.

We discussed how the various scenarios can be distinguished. In all cases, we find that the simultaneous observation of the four channels, in particular nuclear charged and neutral current processes, is fundamental in order to decouple the supernova from the neutrino oscillation physics.

The observed event rates and the event energy spectra of the four classes of events form a set of observables sensitive to the supernova parameters and to the intrinsic neutrino oscillation parameters (θ_{13} and mass hierarchy). We have qualitatively illustrated this with several examples.

In order to understand quantitatively the sensitivity to such parameters, one should study the classification of actual detected events into the four channels and perform a global fit to the observed distributions. Such an analysis will be the subject of a future work [23].

Acknowledgments

We would like to acknowledge T.A. Thompson and A. Burrows for providing data about the neutrino breakout spectra of core collapse supernovae and for useful discussions. We thank G. Martinez-Pinedo, E. Kolbe and K. Langanke for their calculations on the neutrino cross sections for Argon nuclei and for very valuable discussions.

References

[1] K. Hirata *et al.*, *Phys. Rev.* D38 (1988) 448; *Phys. Rev. Lett.*58 (1987) 1490.
R. Bionta *et al.*, *Phys. Rev. Lett.*58 (1987) 1494.

[2] S.Fukuda et al., *Phys. Rev. Lett.*86 (2001) 5656.
SNO Collaboration, *Phys. Rev. Lett.*87 (2001) 071301.
Y. Fukuda et al., *Phys. Rev. Lett.*82 (1999) 2644.
KamLAND Collaboration, *Phys. Rev. Lett.*90 (2003) 021802.
M. Apollonio et al., *Phys. Lett.* B466 (1999) 415.
K2K Collaboration, *Phys. Rev. Lett.*90 (2003) 041801.

[3] A. S. Dighe and A. Y. Smirnov, *Phys. Rev.* D62 (2000) 033007.

[4] G. Dutta, D. Indumathi, M. V. Murthy and G. Rajasekaran, Phys. Rev. D **61**, 013009 (2000) [arXiv:hep-ph/9907372].

[5] K. Takahashi, M. Watanabe, K. Sato and T. Totani, Phys. Rev. D **64**, 093004 (2001) [arXiv:hep-ph/0105204].

[6] K. Takahashi, K. Sato, H. E. Dalhed and J. R. Wilson, "Shock propagation and neutrino oscillation in supernova," arXiv:astro-ph/0212195.

[7] G. G. Raffelt, M. T. Keil, R. Buras, H. T. Janka and M. Rampp, "Supernova neutrinos: Flavor-dependent fluxes and spectra," arXiv:astro-ph/0303226.

[8] K. Takahashi, K. Sato, A. Burrows and T. A. Thompson, "Supernova neutrinos, neutrino oscillations and the mass of the progenitor star," arXiv:hep-ph/0306056.

[9] C. Lunardini and A. Y. Smirnov, "Probing the neutrino mass hierarchy and the 13-mixing with supernovae," arXiv:hep-ph/0302033.

[10] T. Totani, K. Sato, H. E. Dalhed and J. R. Wilson, Astrophys. J. **496**, 216 (1998) [arXiv:astro-ph/9710203].

[11] H. Minakata, H. Nunokawa, R. Tomas and J. W. Valle, Phys. Lett. B **542**, 239 (2002) [arXiv:hep-ph/0112160].

[12] G. Dutta, D. Indumathi, M. V. Murthy and G. Rajasekaran, and heavy water detectors," Phys. Rev. D **64**, 073011 (2001) [arXiv:hep-ph/0101093].

[13] K. Takahashi and K. Sato, mass hierarchy," Prog. Theor. Phys. **109**, 919 (2003) [arXiv:hep-ph/0205070].

[14] ICARUS Collab., "ICARUS. A Second-Generation Proton Decay Experiment and Neutrino Observatory at the Gran Sasso Laboratory", all proposals are available at *http://www.cern.ch/icarus*.

[15] D. B. Cline, F. Sergiampietri, J. G. Learned and K. McDonald, and solar neutrino studies, and a neutrino factory detector," Nucl. Instrum. Meth. A **503**, 136 (2003) [arXiv:astro-ph/0105442].

[16] T.A. Thompson, A. Burrows and P.A. Pinto, "Shock Breakout in Core-Collapse Supernovae and its Neutrino Signature", astro-ph/0211194, submitted to *Astrophys. J.*, 2002.

[17] K. Langanke, P. Vogel and E. Kolbe, *Phys. Rev. Lett.*76 (1996) 2629.

[18] M. T. Keil, G. G. Raffelt and H. T. Janka, "Monte Carlo study of supernova neutrino spectra formation", arXiv:astro-ph/0208035.

[19] A. Bueno, I. Gil Botella and A. Rubbia, "Supernova Neutrino Detection in a liquid Argon TPC", hep-ph/0307222.

[20] G. Martinez-Pinedo, E. Kolbe and K. Langanke (private communication).

[21] W. E. Ormand, P. M. Pizzochero, P. F. Bortignon and R. A. Broglia, *Phys. Lett.* B345 (1995) 343 [nucl-th/9405007].

[22] R. S. Raghavan, *Phys. Rev.* D34 (1986) 2088.

[23] I. Gil Botella and A. Rubbia, in preparation.

[24] Y. Totsuka, *Rep. Prog. Phys.* 55 (1002) 377.

[25] S. Nakamura et al., *Nucl. Phys.* A707 (2002) 561.
S. Ying, W.C. Haxton and E.M. Henley, *Phys. Rev.* D40 (1989) 3211.